Quantification of Medium and Large Debris in the Great Pacific Garbage Patch Using Visual Observations from Aerial Surveys

Technical Report · September 2017

DOI: 10.13140/RG.2.2.10025.29287

Julia Reisser
Minderoo Foundation

Susan Gibbs
South Australian Museum

Leila Fouda
University College London

Quantification of Medium and Large Debris in the Great Pacific Garbage Patch Using Visual Observations from Aerial Surveys

2016 Expedition Report

Date Published: 24 September 2017

Authors: Chandra Salgado Kent[1], Julia Reisser[2], Sue Gibbs[2], Leila Fouda[2], Damien Morales[2], Hendrik Kniest[3]

Affiliations: [1]Centre for Marine Science and Technology, Curtin University (Australia); [2]The Ocean Cleanup (The Netherlands); [3]University of New Castle (Australia)

Acknowledgements: Support was provided by Teledyne Optech, International Air Response, and Moffett Federal Airfield.

Contents

Table of Figures

Table of Tables

1. Introduction

Since 2015, The Ocean Cleanup Foundation (TOC) has been working to quantify the debris in an oceanic plastic pollution hotspot known as the 'Great Pacific Garbage Patch' (GPGP). The first expedition, the '*Mega Expedition*', was conducted in 2015 and quantified ocean plastic in the region using vessels. In particular, the survey produced reliable quantification of plastics less than 0.5 m in length within and around the GPGP region. To better quantify the amounts of ghostnets and other types of large debris (> 0.5 m), The Ocean Cleanup conducted the '*Aerial Expedition*' within the 'Great Pacific Garbage Patch' in October 2016.

The *Aerial Expedition* used visual observation teams and hyperspectral, RGB and infrared sensors installed on the aircraft to detect debris on the ocean surface. This document specifically reports on the visual observations conducted during the aerial surveys in October 2016.

2. Methods

Study Site

Two aerial surveys were conducted within the GPGP area (Figure 1); the first (Flight 1) crossed the region between approximately 141° W and 135° W longitude at around 33.5° N latitude, and the second (Flight 2) crossed the area between 143° W and 138° W diagonally between approximately 30° N and 33° N latitude. Flight 1 was conducted on 2 October 2016 (UTC) and Flight 2 on 6-7 October 2016 (UTC). The distance and bearing of flight paths were constrained to logistical and weather-related considerations.

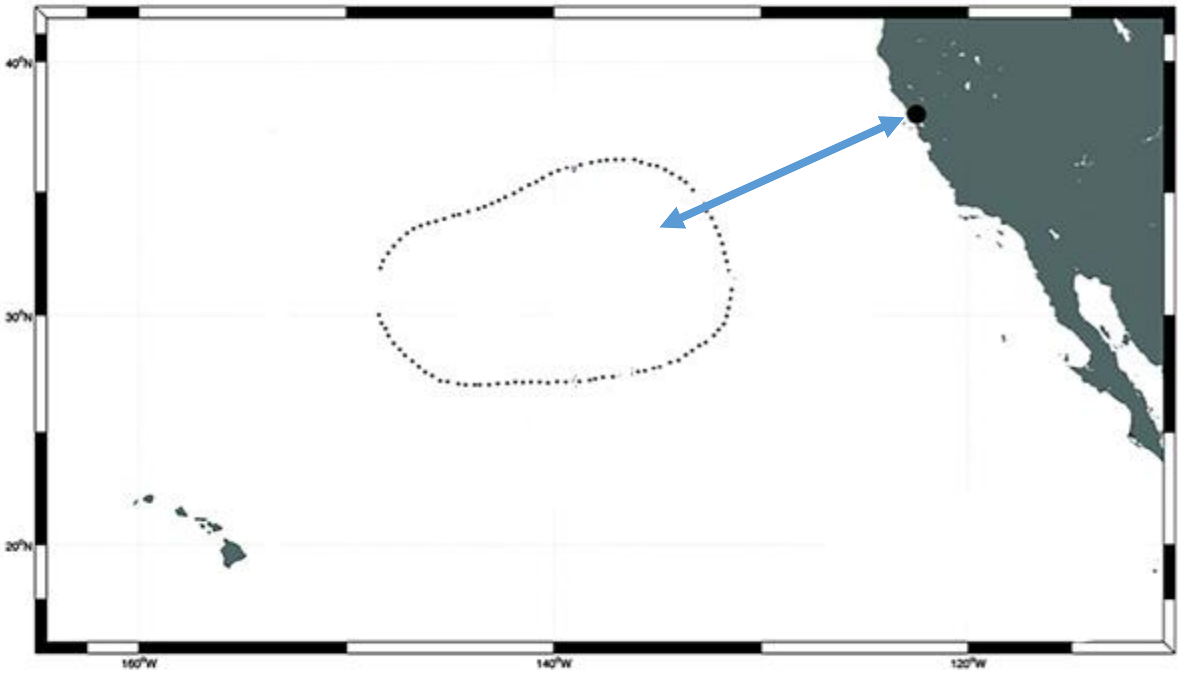

Figure 1. General area of the Great Pacific Garbage Patch in the North Pacific Ocean (black dotted line) and transit route taken by our flights, showing departure location from San Francisco. (blue arrow).

Survey methods

A C-130 aircraft (supplied by International Air Response; Figure 2) was used because it is able to fly over long distances and at low altitude and speeds. This aircraft has been used in debris surveys in other locations in the North Pacific and for search and rescue operations such as the search for debris from the missing Malaysian aircraft MH370. The aircraft flew at high altitude and speed in transit from Moffett Federal Airfield (California, USA) over approximately 2-3 hours to the survey site and 2-3 hours back. However, during the ~2.5-hour surveys the aircraft flew at approximately 400 m altitude and 259.3 km hr^{-1} (140 knots).

Figure 2. Photo of the International Air Response C-130 aircraft used in the expedition.

Each flight was considered a transect, and was designed to be broken into 2 segments separated by a 10-minute break from observations in between 2 hours of continuous 'survey mode'. As such, segment 1 of Flight 1 corresponded to Transect 1.1 (T1.1), segment 2 of Flight 1 corresponded to Transect 1.2 (T1.2), segment 1 of Flight 1 corresponded to Transect 2.1 (T2.1), and segment 2 of Flight 2 corresponded with Transect 2.2 (T2.2). The two transects were designed to optimize ocean models rather than quantify debris abundance using strip transect and distance sampling-based models (Buckland et al. 2004). Analytical approach and assumptions are further discussed below.

The main visual observation surveys took place in the port and starboard open paratroop doors at the sides of the aircraft, using both distance-sampling based surveying and strip transect surveying approaches. Opportunistic debris sighting and with photographic register was also conducted from the port and starboard cockpit windows by a single observer on either side, but the results of this activity are outside the scope of the present report.

Surveys from the paratroop doors were undertaken by four observers; two on the port and two on the starboard side of the aircraft (Figure 3). Observers on the same side of the aircraft were 'blind' to each other – that is, they could not hear or see each other. This was achieved by using different channels for audio communications through headsets used by observers, and by installing a solid aluminum separator between port and starboard observers. Observers were positioned in chairs facing directly out the paratroop doors (at 90° port and starboard from the centerline of the aircraft for port and starboard observers, respectively). Observers were centered so that the left side of the paratroop door was at the same distance from the aft observer as the right side was for the forward observer. The distance each observer was from the bottom edge of the paratroop doors was minimized as much as possible (the observers' feet were at the edges), and was the same for all observers.

Figure 3. Observers positions at the paratroop doors of the C-130 aircraft.

Each observer was paired with a person (the data recorder) dedicated to recording observations reported by the observer. Communications between observer and data recorder were achieved using David Clarke headsets with wind-protected microphones. Headsets were connected to handheld radios with push-to-talk remote switches. In addition, observers were equipped with electronic Haglof digital clinometers fitted with a compass, 7D Mark II cameras with a Canon 70-300mm F/4-5.6 EF USM lens, Canon 10x30 IS II image stabilised binoculars, a notepad and pencil, and polarised sunglasses. Data recorders were equipped with either a laptop computer with external batteries or data sheets for recording observations. All audio transmissions were recorded on a 4-channel Zoom H4NSP audio recorder, with each paired observer and data recorder communications recorded on separate channels.

Data recorders documented the start and end times of transect segments, observers and their positions, and sighting and environmental information in real time. Data recorders equipped with a laptop did so using the positioning software *VADAR* (developed by Dr Eric Kniest at the University of Newcastle, NSW). To ensure that times were recorded correctly, personnel were equipped with watches, and all watches, computers, and cameras were set to UTC and synchronised prior to each flight. In addition, accurate aircraft position and altitude were recorded by the Teledyne Optech team. Also, all instruments (clinometers and cameras) were calibrated before each flight. Cameras were set according to values specified in Table 1.

Table 1. Camera settings used for distance sampling and strip transect surveys.

Setting	**Value**
Mode	Tv
Focus Type	AF
Focus	AI Servo
Shutter	1/1000sec
Aperture	Variable
GPS	Update 1sec
Compass	On
Time	UTC 0 (London)
Quality	RAW
JPEG	No
White Balance	Auto
Shots	Single shot
Evaluative Metering	On

Distance sampling and strip transect surveys were conducted simultaneously by the observers continually scanning the ocean surface for debris and data recorders documenting all information reported by observers. Information collected for distance sampling applications prioritised objects estimated to be larger than 0.5 m in length. When debris that fit this criterion was sighted by an observer, the aircraft side, vertical angle, debris cluster size, debris identification, debris size class, predominant colour, and whether a photo was taken were reported (Table 2). Sightings were called as near as practicable to abeam of observer and data assumes that port sightings were -90º and starboard sightings were 90º from the flightpath heading. This assumption was considered valid given the restricted view of the paratroop doors.

Table 2. Debris information collected for distance sampling-based analyses.

Variable	Description	Levels or Measured Units
Aircraft side	Side the observer was scanning	Port or Starboard
Vertical angle	Angle measured from the horizon down to the object using the Haglof digital clinometer	Degrees (instrument accuracy was 2.5 degrees)
Cluster size	Number of debris objects in the cluster	Number counted floating within close proximity of each other (1 if it was a single item)
Debris Identification	Type of debris	'Net', 'Rope', 'Container', 'Float', 'Other', 'Unknown'
Debris size class	Qualitative estimates made by observers (by eye)	'Small' was estimated to be < 0.5m, 'Medium' was 0.5 - 1m, 'Large' was 1 - 5m, and 'Huge' was >5m in length
Predominant colour	The colour perceived to predominate the object	Colour (if multi-coloured with no predominant colour, then 'multi-coloured' was reported)
Short description	Any other notable features	Text corresponding to the observation
Photos taken	Whether a photo was taken of the object or not	'Yes' or 'No'

For the strip transect approach, traditional approaches to strip transect surveying was not possible. This was a result of the large number of debris present, making it impossible to report all objects within a designated range of the aircraft. Instead, 'sample' photographs were taken with the camera lens set at 70 mm and the bottom of the field of view aligned with the bottom edge of the aircraft paratroop doors. Sample photos were taken as close to every 5 minutes as possible in Flight 1, and adjusted to approximately every 2 minutes in Flight 2. The data collected are reported on here. However, abundance estimation and size class, debris type, and debris colour distributions from strip surveys are not presented here as they were undertaken as an addition to the original scope of work. These data are available for comparative abundance estimation.

During systematic surveys conducted from the paratroop doors, each observer reported weather conditions within their field of view that could affect detection of objects. Weather conditions were reported at the start of each transect, when conditions changed and each hour while on survey. Weather conditions included, cloud cover, glare intensity, glare direction, turbidity, sea state (Beaufort scale), and visibility (Table 3). Wind speed and wind direction were obtained when measured by the pilots.

Table 3. Weather conditions recorded during systematic surveys.

Variable	Description
Glare intensity	A scale of 0 to 3 was used, with 0 corresponding to no glare and 3 to the most intense glare.
Glare direction	The glare direction with bearings (using the compass in the clinometers) on the left and right side of the glare was reported. If the glare is equal in all directions / spread across the entire field of view, then '*dispersed*' was reported.
Sea state	The Beaufort scale was used to describe the sea state condition on a scale of 0 to 12, with 0 corresponding to a glass-off and 4 corresponding to breaking waves with white horses beginning to form (see *Appendix B*). Surveys were conducted in Beaufort conditions less than 4/5.
Turbidity	Turbidity was recorded on a scale ranging from 0 to 3, with 0 corresponding to highly transparent water and 3 corresponding to water in which objects could not be seen once submerged.
Cloud Cover	Cloud cover was recorded as the percent of the sky within the field of view covered with cloud.
Visibility	Visibility was recorded as the vertical angle down from the horizon to where there was clear visibility (using clinometer).

Data written in data sheets were transferred to electronic spreadsheets, and all data and photographs were backed up onto two external hard drives at the end of each flight. All data need to be downloaded and backed-up. Data QA/QC was conducted as soon as possible after the flights.

Image processing

Photographs taken during systematic surveys were used for debris identification and measurement. All photographs of debris reported during distance sampling surveys were processed for comparison to information reported by observers during the surveys. For strip transect surveys, a subsample of images was processed. The subsample consisted of a photograph every 5-minute period (5-min block). This ensured that a high-quality image was available from each observer position within each time period (equal effort).

Image processing first involved ranking images by their quality using criteria and ranking scales in Table 4.

Table 4. Image quality ranking.

Criteria	Scale
Quality of image (clarity & contrast)	poor, fair, good, or excellent
Glare intensity	0 (no glare) to 3 (most intense glare), as per aerial observations
Glare coverage	qualitative estimate of percentage of the ocean surface with glare
Cloud Cover	qualitative estimate of percentage of image with clouds obscuring the ocean surface
Aircraft or sky in photo	qualitative estimate of percentage of photo with aircraft or sky captured
White water (white caps, white horses)	many, numerous, scattered, or none (these descriptions are similar to descriptions Beaufort scale, but with white caps and white horses combined)
Sunbursts	present (1) or not present (0)
Item distinctiveness (combination of clarity, contrast, item orientation, position in water, colour, type, etc.)	poor, fair, good, or excellent
Unidentifiable white pixel areas	0= none, 1= scattered or a small number, 2= numerous, 3= many

Debris identification and color were categorized as during distance sampling surveys. Measurements of debris sizes were undertaken by using a measuring tool in Photoshop Elements 11, and correcting the measured size using the following parameters: lens zoom applied, the altitude of the aircraft, and the declination angle down from the horizon the camera was angled at. To calculate debris sizes, images were taken of an object of known length (1 m) at the range of focal lengths used (most at 70 mm, but ranging up to 300 mm). The ruler tool was used in Adobe® Photoshop® Elements 11 to calibrate the dimensions of the 1 m calibration object within the image to the length of the object in real life (1 m). The calibrated ruler image was then used to measure the length and width of debris captured in the images at their longest dimensions. All calibrations were undertaken assuming a 400-m height of the aircraft. However, corrections were made for variation in flying height and inclination angle to the object relative to a 0° set at a vertical plane straight down from the aircraft. The following equations were used for the additional corrections:

$$Angle\ of\ inclination = Declination - 90 \qquad \text{(Eq 1)}$$

$$Distance\ to\ the\ object = \frac{Actual\ aircraft\ height}{\cos(Angle\ of\ inclination)} \qquad \text{(Eq 2)}$$

The proportional difference between the calculated distance to the object and the assumed 400 m was used to scale up the height and length measurements of the debris extracted from Photoshop.

The distortion resulting from the image not being taken perpendicular to the sea surface (Figure 4) was assumed to have a negligible effect on size class categorisation for the purposes of this report.

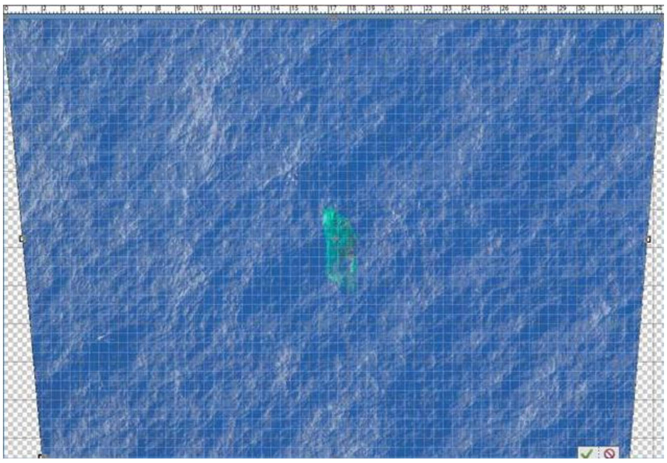

Figure 4. Example of distortion resulting from photographs taken at an angle not perpendicular to the sea surface.

Distance sampling abundance estimates of debris

Mark recapture distance sampling (MRDS; Buckland et al. 2004; Buckland et al. 2015) includes a range of methods used for estimating the density and abundance of objects surveyed by teams of double blind observers (observers measuring the same area, but that are 'blind' to each other visually and acoustically). Generally, objects are biological populations, however, the methods can be used for debris. Distance sampling allows for observers to sample objects while moving along a line or transect. The method assumes that all objects are detected along the transect (at range 0 from it), and drops away with range away from the transect. A detection function with perpendicular range away from the transect is fit, and the undetected objects at range corrected for using the estimated probability of detection at range. Thus, the detection function is used to estimate the number of objects missed, which is used to produce estimates of absolute abundance. Using 'double-blind' teams allows for perception bias by observers to be corrected. Mark recapture distance sampling (MRDS) allows the integration of both of these sampling biases to be estimated and abundance of objects to be estimated based on corrections of objects that were missed.

Abundance estimates were made using Distance in R as described in Miller et al. (2016). Distance uses the package mrds (Laake et al. 2015) designed for mark-recapture distance sampling (Burt et al. 2014), requiring a complex data structure to perform analyses. Models were fit using half-normal, hazard-rate, gamma, and uniform key functions with cosine, Hermite polynomial and simple polynomial adjustments, and covariates including, debris type, debris size, debris colour, Beaufort sea state, glare, cloud cover, side of the aircraft and interactions of these with distance. The Mark Recapture models were fit with the covariates of distance and the interaction of distance with observer. Model selection were carried out based on the most parsimonious model that reduced the AIC scores by more than 2 units. Diagnostic tools included Q-Q tests, and goodness of fit tests (Chi-squared, Kolmogorov-Smirnov, and Cramer-von Mises tests).

3. Results

A total of 1,129 km during 4.17 hours were surveyed during two survey flights. Flight 1 was conducted on Monday, 2 October 2016, and covered a survey transect 563.6 km long (Transect 1) during 2.17 hours (between 19:04 and 21:14 UTC; Table 5). Flight 2 was conducted between Thursday, 6 and Friday, 7 October 2016, and included a transect 565.4 km long (Transect 2) during 2.18 hours (Table 5). Transect 2 was broken into two segments (segments 1 and 2) separated by ~10 min break. Segment 1 was surveyed over a period of 1.88 hours (between 22:18 on the 6th and 00:11 on the 7th October UTC) and Segment 2 over 0.30 hours (between 00:20 and 00:38 on the 7th October UTC). The average speed of the aircraft during survey mode was 259.7 km hr^{-1} on 2 October 2016 (Transect 1) and 259.4 km hr^{-1} on 6-7 October 2017 (Transect 2).

Table 5. Aerial survey effort for visual observations of marine debris in the Great Pacific Garbage Patch on 2 and 6-7 October 2016.

Date	Survey transect & segment (transect.segment)	Start / End	Latitude	Longitude	Time (UTC)	Duration (hrs)	Length (km)
2/10/2016	1.1	Start	33.49804	-141.00817	19:04:05	2.17	563.6
		End	33.49697	-134.93638	21:14:01		
6/10/2016	2.1	Start	30.21098	-143.60820	22:17:45	1.88	488.8
7/10/2016		End	32.42226	-139.1644	00:11:00		
7/10/2016	2.2	Start	32.60904	-138.7842	00:20:33	0.30	76.6
		End	32.95611	-138.08090	00:38:12		

Transect 1 was flown at a mean bearing of 88.33° from true north, while Transect 2 was flown at a mean bearing of 58.45° from true north.

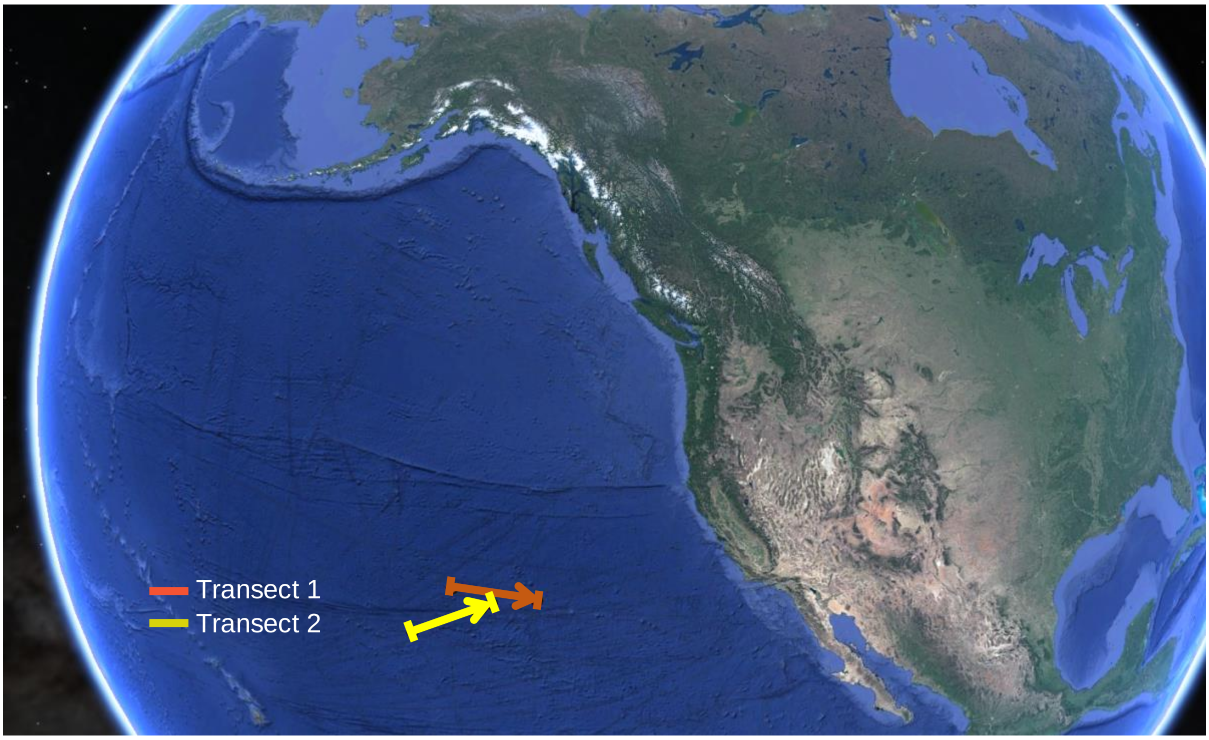

Figure 5. Location, coverage, and direction of aerial survey Transects 1 and 2 in the Pacific Ocean (Source of map: Google Earth).

The height of the aircraft varied, commencing at low altitude proceeding lift off in San Francisco, high altitude (between 6,000 and 7,000 m) during transit to the start position of the survey transect, low altitude during surveys (at approximately 400 m), and high-altitude on transit back to San Francisco (Figure 6).

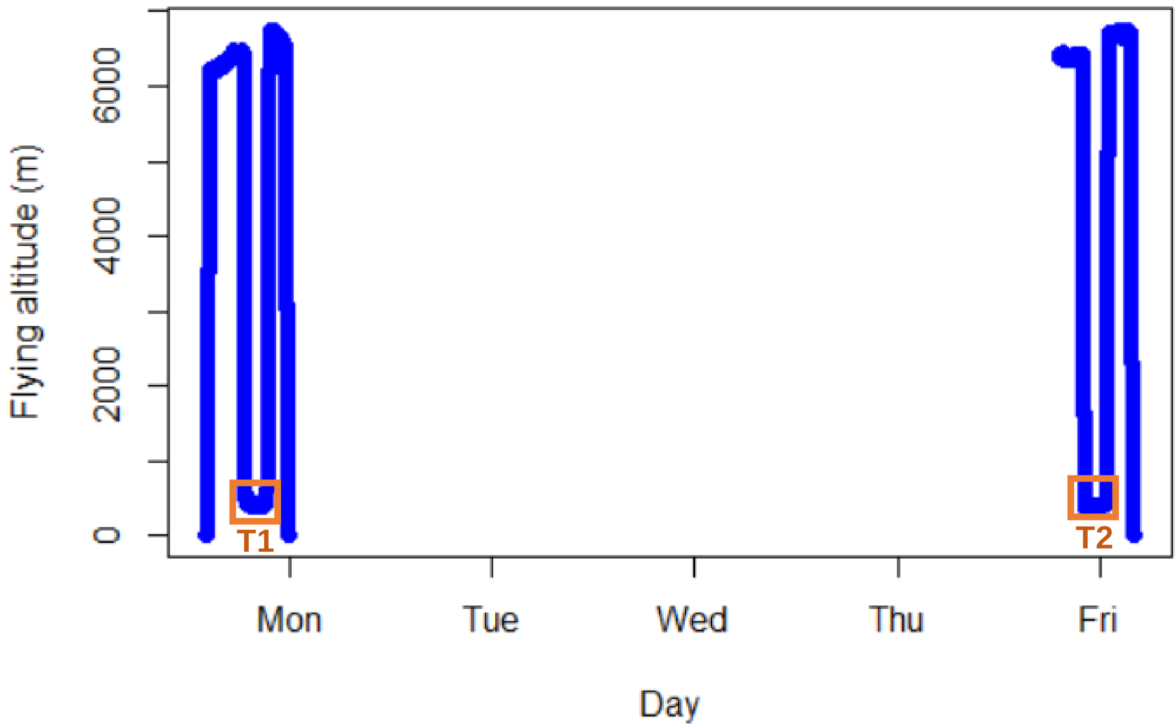

Figure 6. Aircraft altitude during flights on Monday 2 and Thursday 6 to Friday 7 October 2016 (orange squares indicate the periods during surveys of Transect 1 (T1) and Transect 2 (T2)).

While 400 m was the target altitude of the aircraft during surveys, the altitude ranged between 384 and 447 meters during Transect 1 and 353 and 431 meters during Transect 2 (Figure 7).

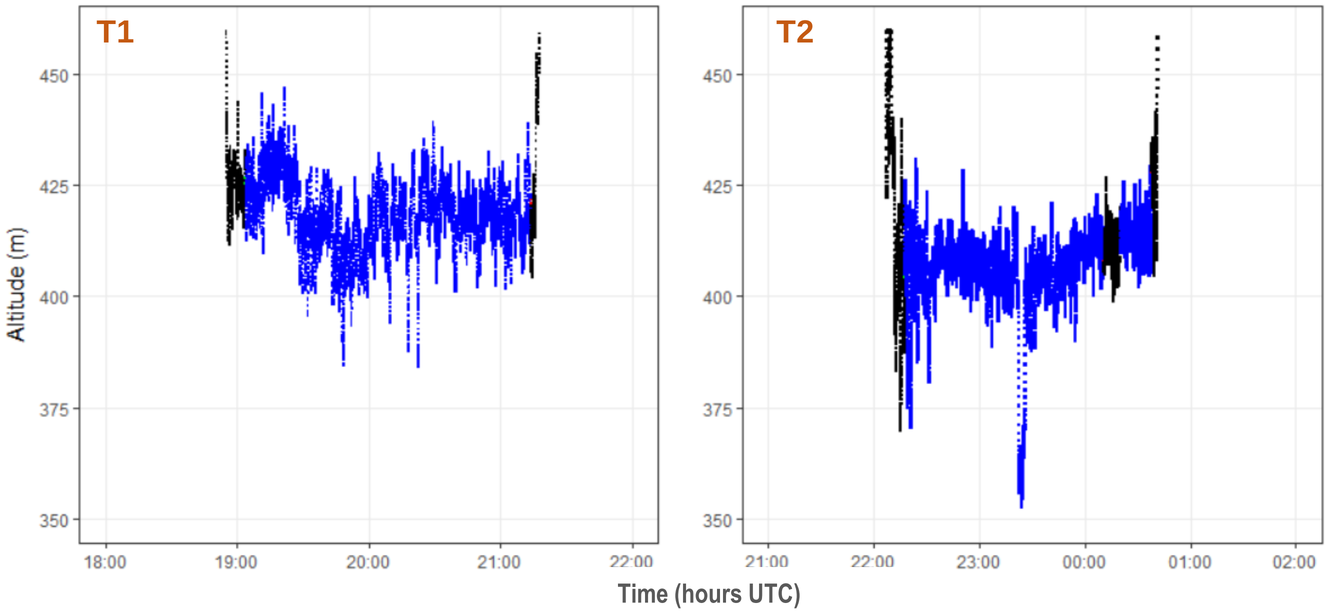

Figure 7. Aircraft altitude during Transects on Monday 2 (T1) and Thursday 6 to Friday 7 (T2) October 2016 (blue indicates on-transect periods and black represents off-transect periods).

Debris size estimates

During surveys, observers identified the greatest number as huge followed by large, and even reported some medium and small objects (Figure 8). The number of huge items was 126 (41%), large was 96 (31%), medium was 49 (16%), small was 8 (3%), and 30 (10%) was unknown.

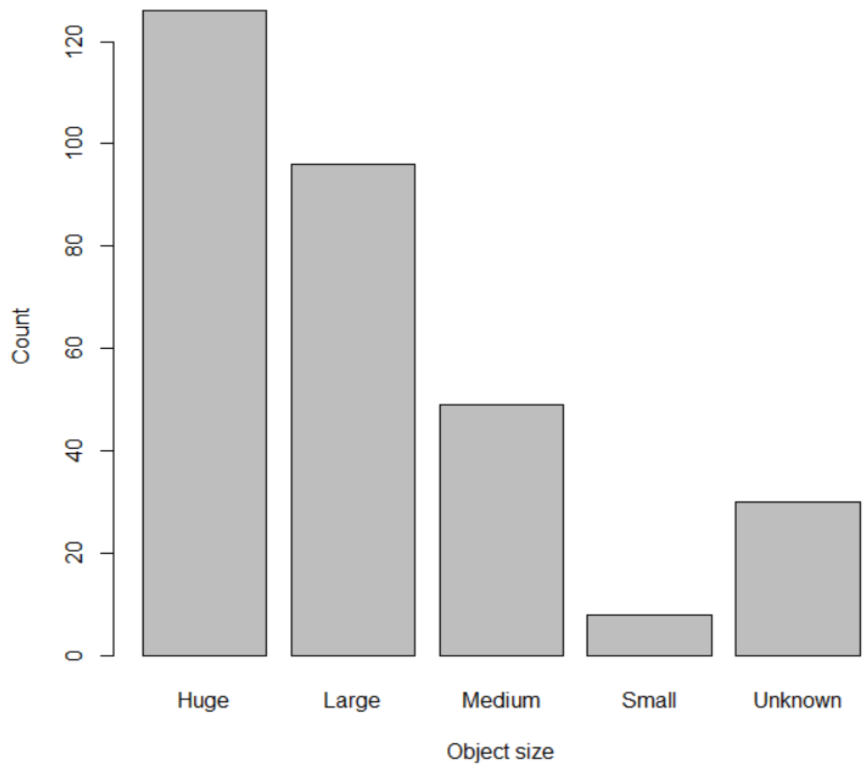

Figure 8. Debris sizes reported by all observers on Transects 1 and 2 during aerial surveys in the Great Pacific Garbage Patch on 2 and 6-7 October 2017.

Debris sizes observed directly during surveys varied from those measured from photographs taken of the same objects. Sizes based on visual qualitative assessment were generally larger than those based on measurements in photographs (Figure 9). While most items were reported as 'huge' (> 5 m) when assessed qualitatively by sight, these corresponded to the 'large category (1-5 m) when measured in photographs. Likewise, many considered to be 'large' qualitatively were 'medium' (0.5-1 m) when measured in photographs. The greatest numbers were large, and even reported some medium and small objects (Figure 8). Of those measured, the number of large debris dominated (43%), followed by medium (32%), small (24%), and huge (1%).

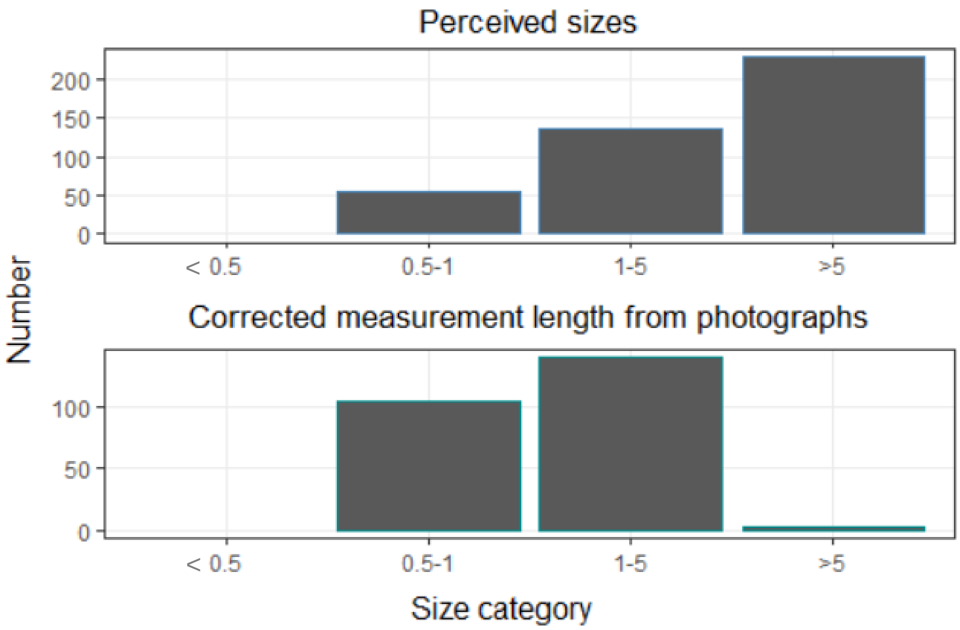

Figure 9. Debris sizes reported by all observers on Transects 1 and 2 during aerial surveys in the Great Pacific Garbage Patch on 2 and 6-7 October 2017.

Photograph-based measurements of debris lengths (the longest aspects of each debris) based on the assumed 400 m flying altitude had errors up to 25 cm smaller than the corrected sizes.

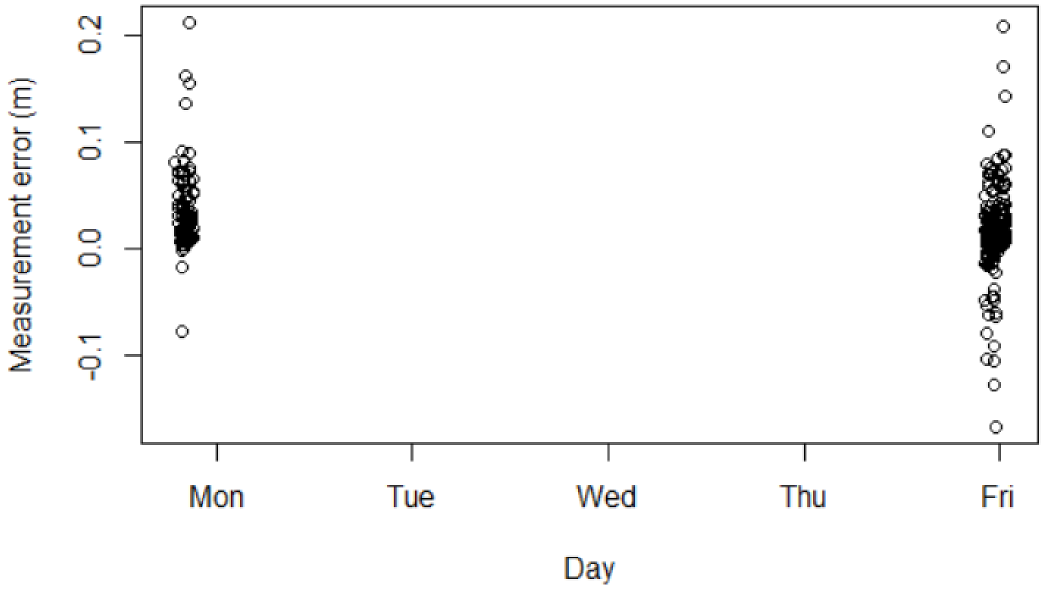

Figure 10. Debris length errors for debris measured from photographs on Transects 1 and 2 during aerial surveys in the Great Pacific Garbage Patch on Monday 2 and Thursday/Friday 6-7 October 2017 if an altitude of 400 m were assumed.

However, corrections did not change the overall distribution of size classes.

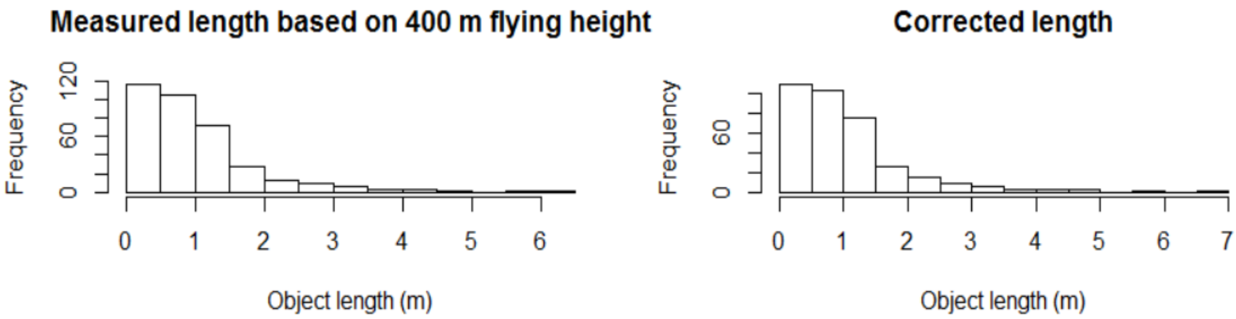

Figure 11. Debris size distribution measured from photographs taken on Transects 1 and 2 during aerial surveys in the Great Pacific Garbage Patch on 2 and 6-7 October 2017; a) assuming 400 m flying altitude, and b) corrected based on measured altitude.

Debris types and colours

The greatest number of debris type detected were nets, followed by containers and other types outside the main categories, then by unknown objects and ropes (Figure 12). Floats were the fewest reported. While there were large numbers of floats present, these were less frequently reported due to their smaller sizes. Debris type reported during visual observations and from inspecting photographs of the objects were mostly consistent. The greatest variation was in the total number of objects available to obtain information from, with over 30% more from sightings than photographs (since photos take time to obtain; Table 6). However, if the object was photographed, there was a great reduction in number of debris of unknown type and larger number in 'other' due to greater time available to view the object (Figure 13).

Table 6. Numbers and percentages of marine debris types reported upon sighting and inspection of photographs obtained when sighted during surveys in the Great Pacific Garbage Patch on 2 and 6-7 October 2016.

Method of identification	Net	Rope	Container	Float	Other	Unknown	Combinations of Net, Ropes, Floats	Total
Number								
Sighting during survey	95	29	18	12	14	143	0	311
Inspection of photograph taken	83	21	1	5	30	39	7	186
Percent								
Sighting during survey	31	9	6	4	5	46	0	
Inspection of photograph taken	45	11	1	3	16	21	4	

The most common colour of debris was reported to be white, followed by blue, green and grey.

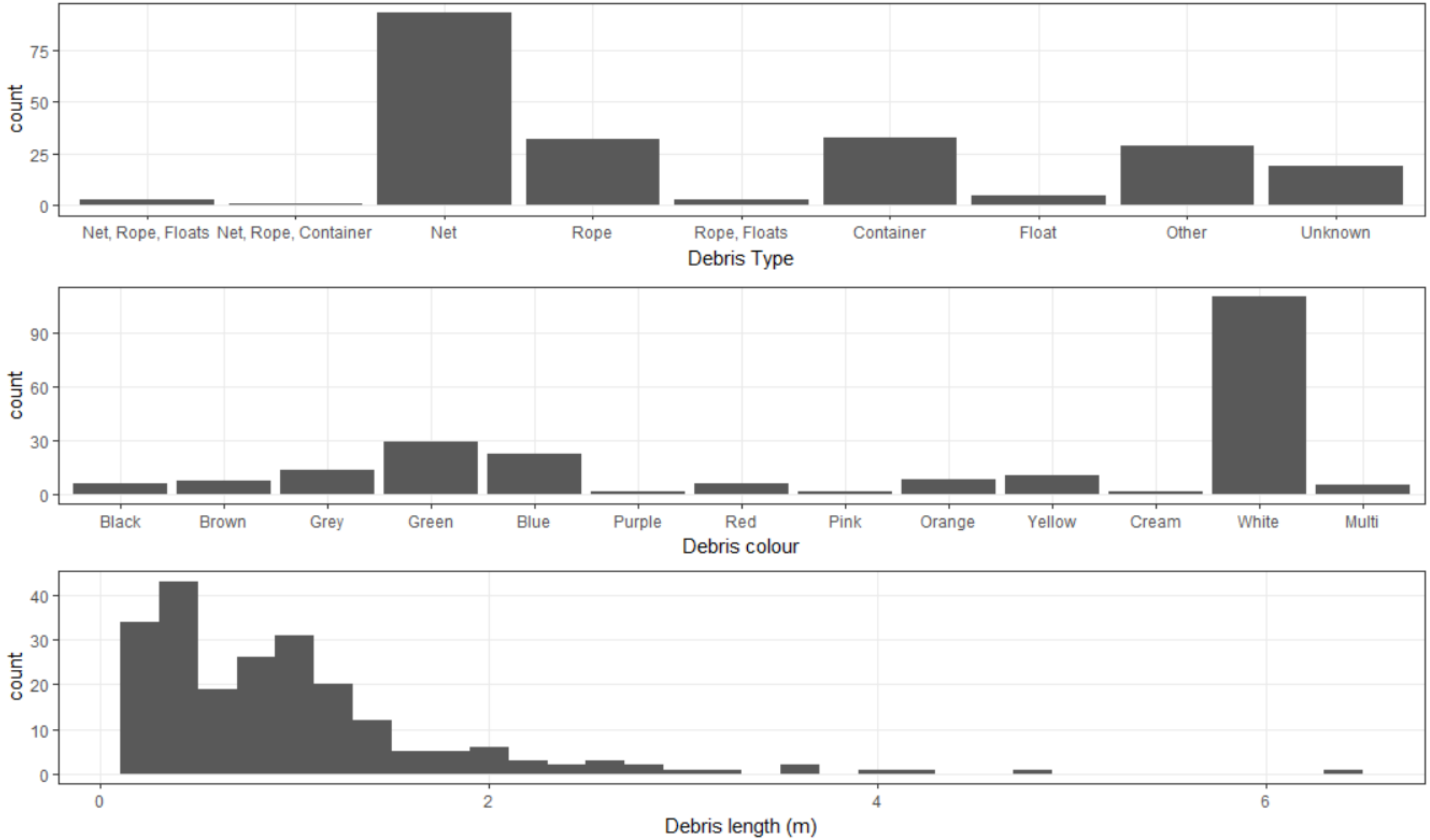

Figure 12. Debris types and colours reported by all observers on Transects 1 and 2 during aerial surveys in the Great Pacific Garbage Patch on 2 and 6-7 October 2017.

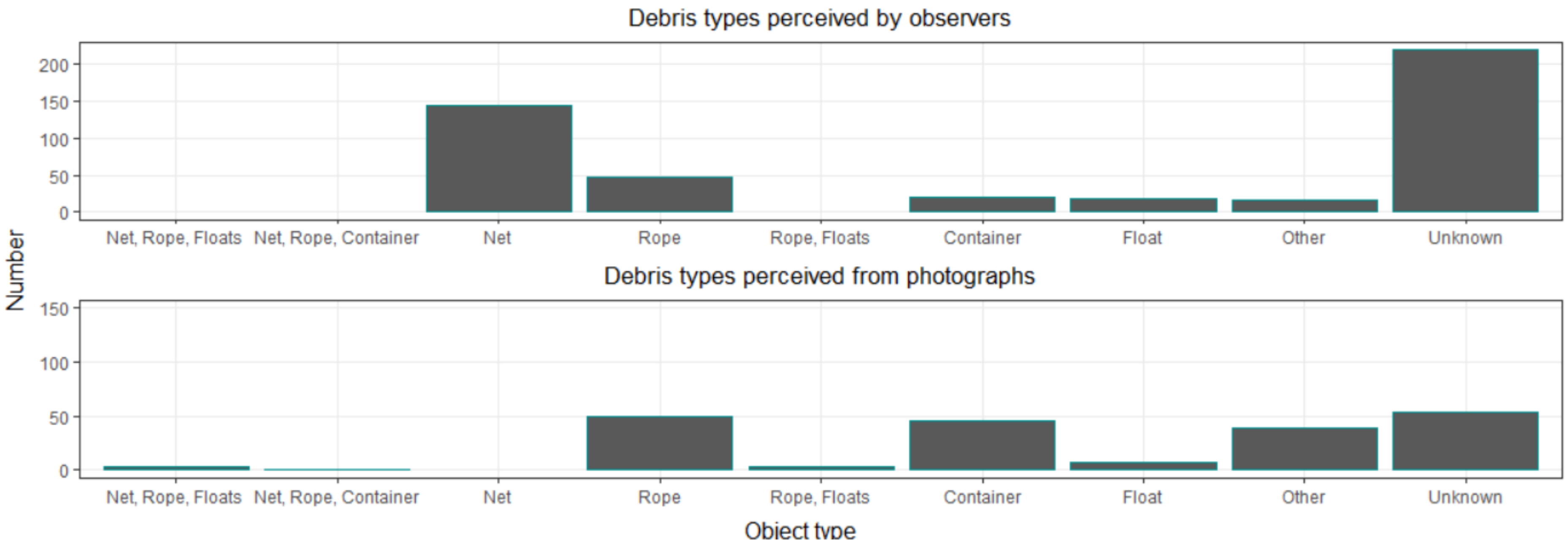

Figure 13. Debris types perceived by all observers directly and from photographs taken during aerial surveys of Transects 1 and 2 in the Great Pacific Garbage Patch on 2 and 6-7 October 2017.

Debris abundance estimates

A total of 313 objects that were perceived to be large or huge sizes (1 - 5m, and >5m in length, respectively) of debris were recorded visually by all for observers during the aerial surveys; 151 during the survey of Transect 1 and 162 during Transect 2. Many smaller debris were sighted but not reported due to the overwhelming number of these present.

Overall, more debris were detected by forward observers than port observers. The forward observers were more experienced that the aft observers. On Transect 1 more debris were detected on the port side, while on Transect 2 more debris were detected on the starboard side of the aircraft (Table 7).

Table 7. Aerial survey effort for visual observations of marine debris in the Great Pacific Garbage Patch on 2 and 6-7 October 2016.

Transect	Side	Position	Number of debris detected
1	Port	Forward	101
		Aft	38
	Starboard	Forward	12
		Aft	0
2	Port	Forward	26
		Aft	18
	Starboard	Forward	67
		Aft	51

Number of detections was related to sighting conditions and field of view of observers, which varied in port and starboard and forward and aft positions. In particular, the number of detections was associated with glare, Beaufort, and visibility conditions. Numbers of detections dropped significantly in glare scores above 1 and Beaufort conditions greater than 2 (Figure 14). Glare was particularly intense on the starboard side of the aircraft on Transect 1. While cloud coverage in the sky was not related to number of debris detected, unexpectedly clouds below the aircraft were encountered during Transect 2, and obscured the view of all observers during part of the survey.

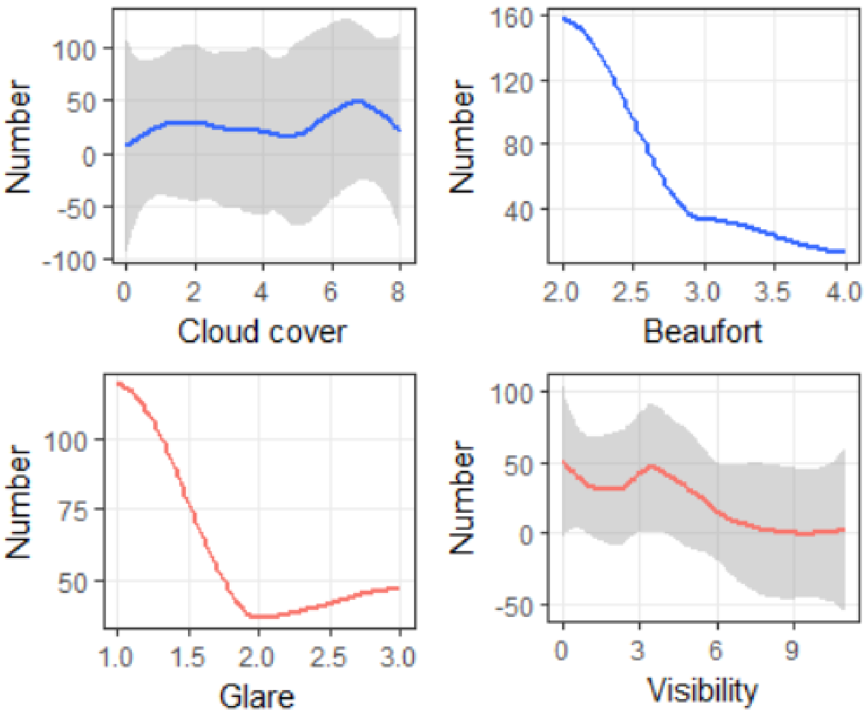

Figure 14. Number of debris detected in different sighting conditions during aerial surveys in the Great Pacific Garbage Patch on 2 and 6-7 October 2017 (the lines are loess smoother with 95% CI indicated in grey shading where they could be calculated).

Debris were observed throughout the transects, however there were some areas where greater numbers were detected (Figure 15).

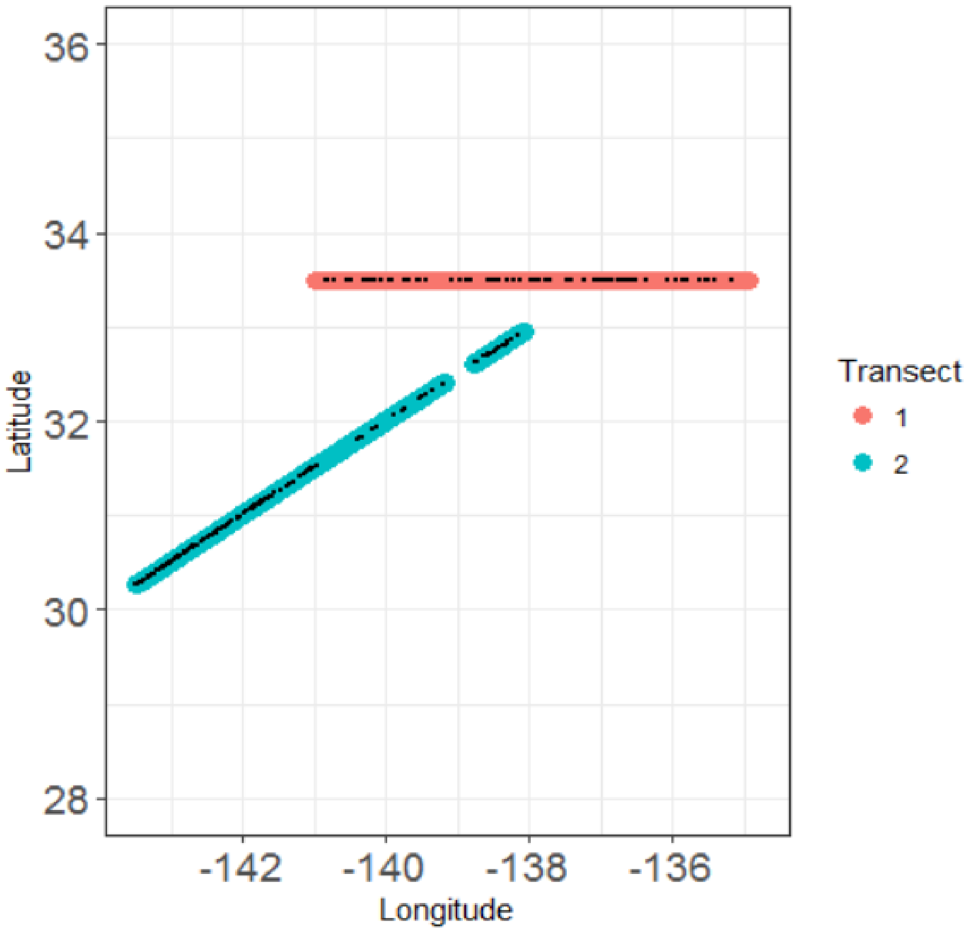

Figure 15. Location of objects sighted along Transects 1 and 2 by all observers during aerial surveys in the Great Pacific Garbage Patch on 2 and 6-7 October 2017.

To assess distribution of debris, each Transect was split up into 20 equal segments (Figure 16). Transect 2, actually had 21 segments since the 10-minute observer rest period broke up the 17th segment into two. Transect 1 segments were 28.18 km each, while Transect 2 segments were 28.27 km each.

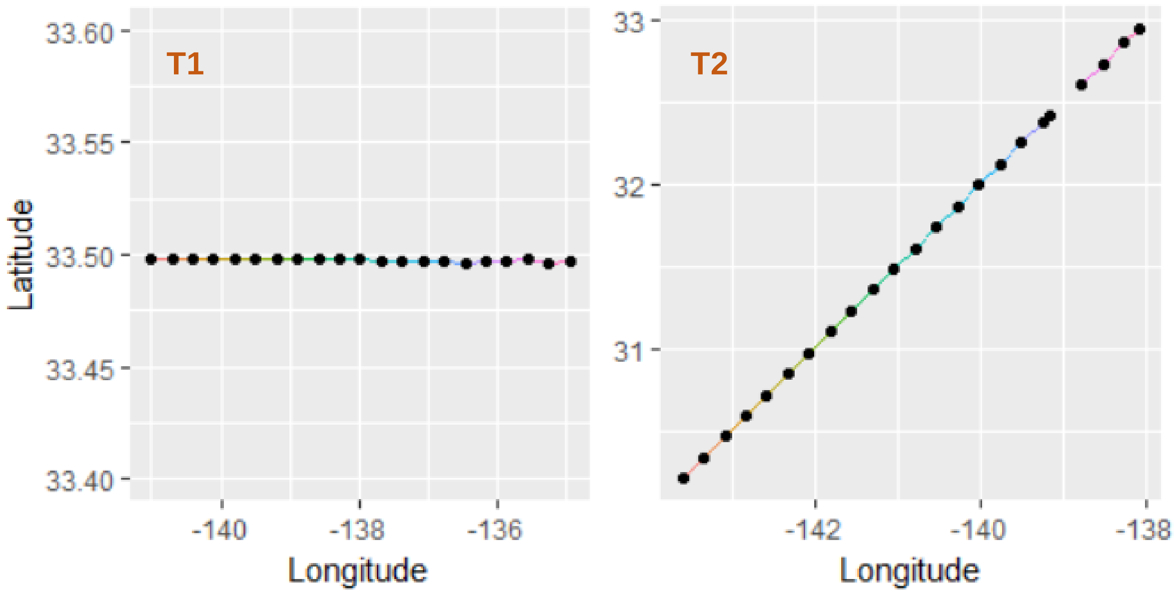

Figure 16. Great Pacific Garbage Patch aerial debris survey transects 1 (T1) and 2 (T2) split into 20 segments of equal length.

The number of debris detected was variable among segments, with a drop off in sightings at the end of Transect 1 and in the middle and towards the end of Transect 2, except for the very last segment which had high detections (Figure 17). Beaufort condition as an example of its association with the number of debris detected in port and starboard and forward and aft positions has been overlaid as a Loess smoother (with 95% CI where possible to calculate) in Figure 17. Clouds below the aircraft obscured the view of the ocean between segments approximately between 9 and 15. In 11 and 12 debris detections dropped significantly.

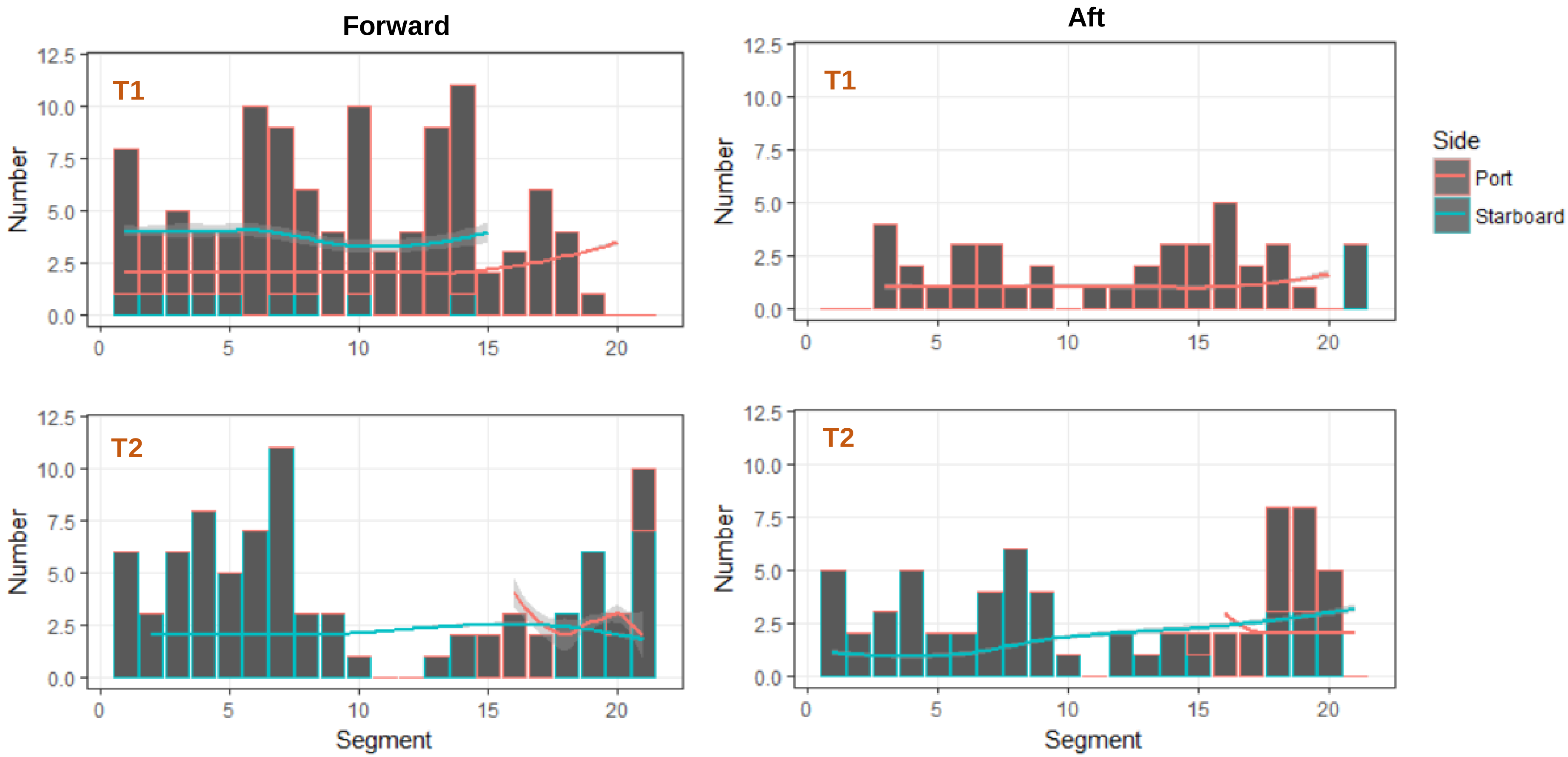

Figure 17. Number of debris detected by port and starboard forward and aft observers within the 20 segments of Transects 1 and 2 (T1 and T2, respectively) surveyed during flights in the Great Pacific Garbage Patch on 2 and 6-7 October 2017. Mean Beaufort conditions are indicated with a loess smoother with 95% CI.

Absolute abundance of debris per segment and within each transect area was estimated using distance sampling approaches. First the detection range of debris was assessed, and a function fitted to the data. Often the targetted height of the aircraft, which in this case was 400 m, is assumed to be accurate. However, due to the relatively high variability in aircraft altitude, a correction to all distances based on measured altitude (provided by Teledyne Optech team) was applied.

Detection peaked between 300 and 400 m from the aircraft (Figure 18). A blind spot was evident at ranges closer than 300 m. Detection dropped off more steeply at range in distances corrected by the measured aircraft altitude (Figure 18). Virtually no detections were made at distances beyone 1.2 km from the aircraft.

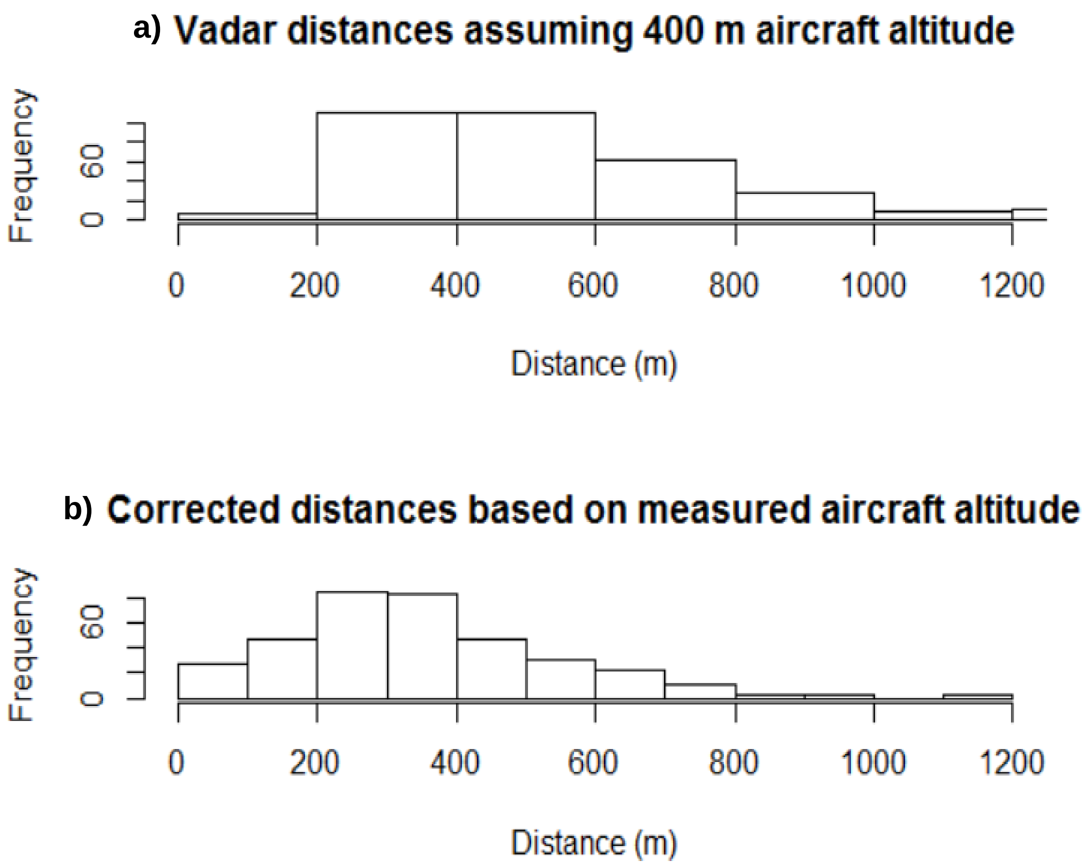

Figure 18. Detection ranges of perceived large and huge debris detected by all observers on Transects 1 and 2 during aerial surveys in the Great Pacific Garbage Patch on 2 and 6-7 October 2017; a) assuming 400 m altitude and b) corrected using measured altitude.

Expected errors using the assumed 400 m altitude could be expected to range up to as ~800 m (Figure 19).

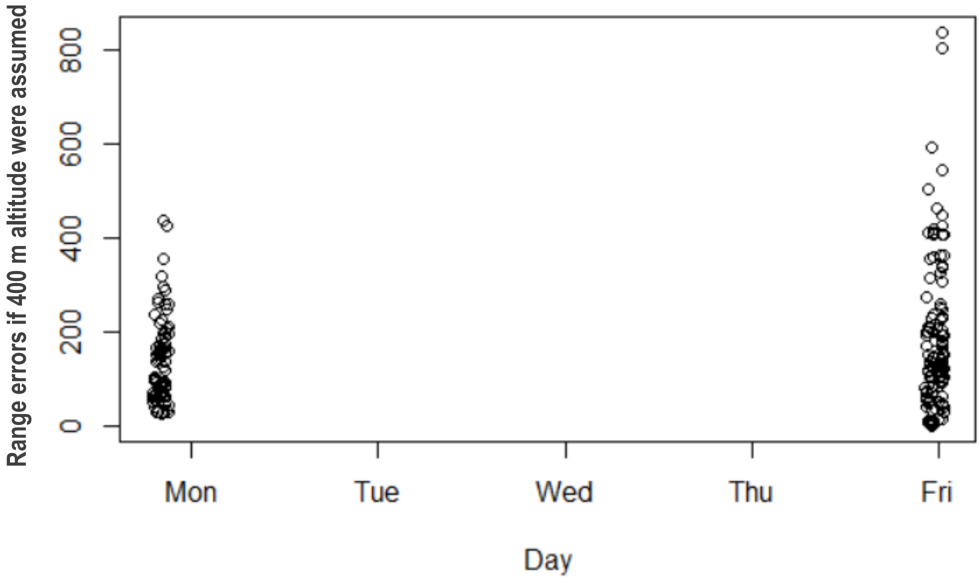

Figure 19. Detection range errors for perceived large and huge debris detected by all observers on Transects 1 and 2 during aerial surveys in the Great Pacific Garbage Patch on Monday 2 and Thursday/Friday 6-7 October 2017 if an altitude of 400 m were assumed.

Distance sampling estimates were undertaken for all debris (small, medium, large, and huge class sizes combined), medium size class debris (0.5 to 1 m) and large size class debris (1 m to 5 m) based on the longest lengths derived from photos. The huge size class was not included in its own analysis as there were only three objects which are insufficient observations for distance sampling-based estimates. Modeling was undertaken by removing 80 of the 297 debris objects that did not have distances measurements associated with them. Thus 26.9% of items are not accounted for in the abundance estimates, but abundance estimates were corrected for these missed items by multiplying values by 1.269.

Based on corrected detection ranges, a detection function with left and right truncations of 300 m and 1.8 km, respectively, were applied to trim away effects from the blind spot near the aircraft and very low detections at larger ranges. The resulting half strip width was 1.5 km. Areas surveyed during Transects 1 and 2 were calculated to be 1127.3 and 1130.8 km^2, respectively. Hereforeward, Transects 1 and 2 are called the ‘North’ and ‘South’ Regions, respectively, to limit confusion by keeping within the Distance Sampling terminology (Table 8).

Table 8. Region, area, area covered, and effort computed from Distance Sampling models.

Region	Area (km^2)	Covered Area (km^2)	Effort (km)
North	1127.28	1690.92	563.64
South	1130.78	1611.36	537.12
Total	2258.06	3302.28	1100.76

Model goodness of fit tests

The best fit MRDS models (lowest AIC) had detection functions either with a half-normal or hazard-rate key function on its own or with Glare as a covariate (Table 9). Beaufort, cloud cover, side of the aircraft, debris type, and debris colour were not significant as covariates. Goodness of fit tests and Q-Q plots indicated good fit (Table 10 and Figure 20).

The estimated probability of detecting items due to dropping detections with distance ranged from 0.35 for medium to 0.27 for large debris, and 0.26 for all objects combined (Table 9). The probability of debris being detected by observers (perception bias) was 0.54 for medium and 0.71 for large debris, and 0.53 for all debris size classes combined (Table 9, Figure 21-Figure 23). The overall model detection probabilities were 0.19 for medium and large debris, and 0.14 for debris of all size classes.

Table 9. Summary of best fit MRDS models.

Model	DS model (hn = half-normal, hr = hazard-rate)	MR model	Truncation (m)	AIC	Num Obs	Average probability (p)	Estimate	SE	CV
All debris	cds(key = "hr")	~glm(~observer*distance)	Left=300 Right=1800	483.36	268	Detection function p	0.26	0.02	0.06
						Perception p	0.53	0.07	0.14
						Model p	0.14	0.02	0.15
Large sized debris	~cds(key = "hn")	~glm(~distance*observer)	Left=300 Right=1800	120.74	87	Detection p	0.27	0.02	0.09
						Perception p	0.71	0.11	0.15
						Model p	0.19	0.34	0.18
Medium sized debris	cds(key = "hn", formula=~Glare)	~glm(~distance*observer)	Left=300 Right=1800	126.29	72	Detection p	0.35	0.03	0.09
						Perception p	0.54	0.15	0.27
						Model p	0.19	0.05	0.31

Table 10. Goodness of fit tests for MRDS models.

Model	Method	Test statistic	P	df
All debris	MR total chi-square	21.29	0.17	10
	Total chi-square	25.29	0.03	14
	Distance Kolmogorov-Smirnov test	0.023	0.99	-
	Distance sampling Cramer-von Mises test (unweighted)	0.019	0.99	-
Large sized debris	MR total chi-square	7.480	0.28	6
	Total chi-square	9.537	0.39	9
	Distance Kolmogorov-Smirnov test	0.066	0.83	-
	Distance sampling Cramer-von Mises test (unweighted)	0.055	0.89	-
Medium sized debris	MR total chi-square	2.28	0.32	2
	Total chi-square	3.55	0.17	2
	Distance Kolmogorov-Smirnov test	0.12	0.25	-
	Distance sampling Cramer-von Mises test (unweighted)	0.22	0.24	-

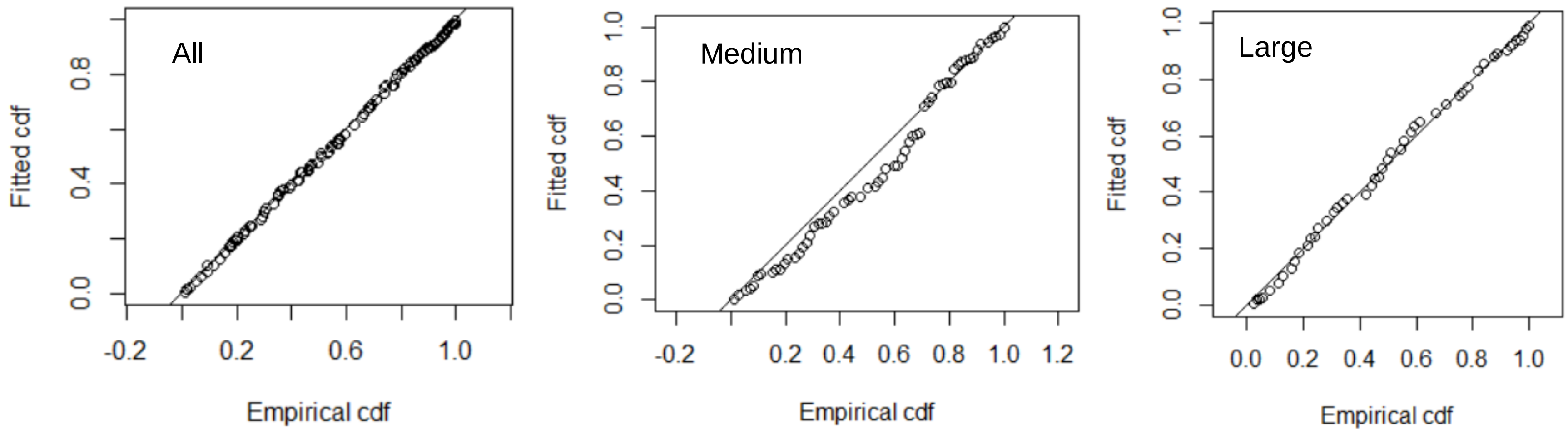

Figure 20. Q-Q plots for MRDS models for All, Medium and Large sized debris.

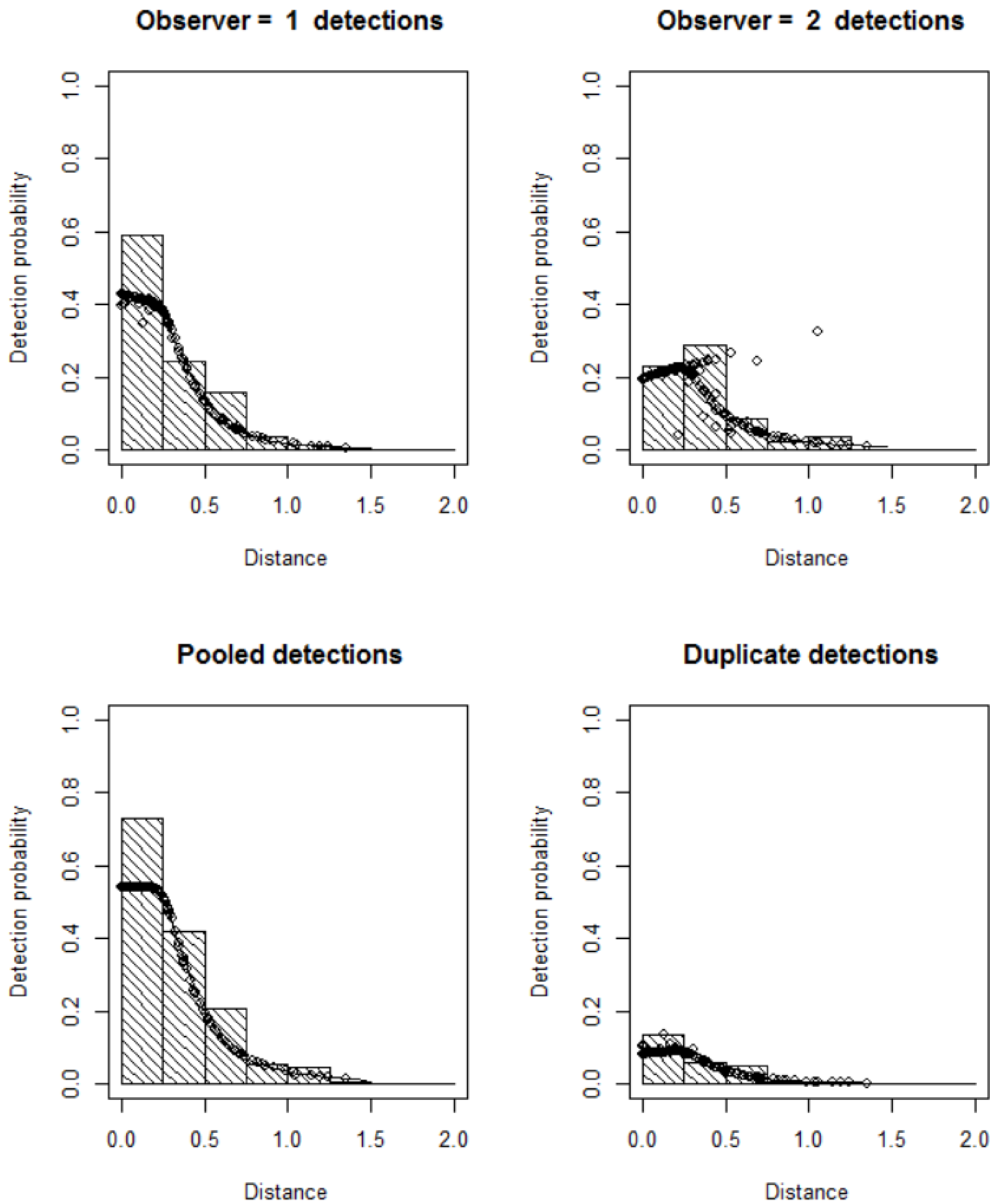

Figure 21. Detection probabilities for MRDS for all debris.

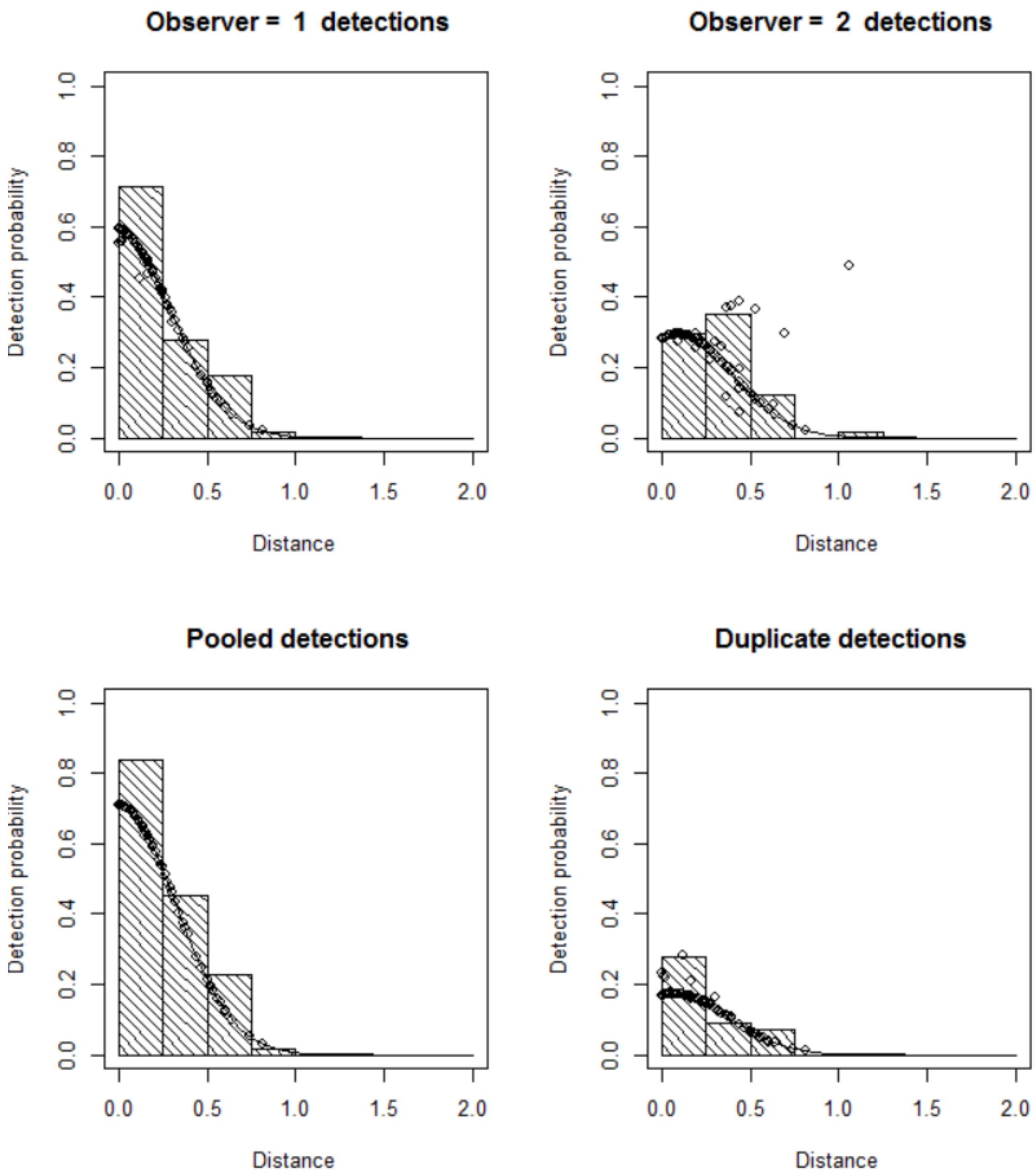

Figure 22. Detection probabilities for MRDS for Large debris.

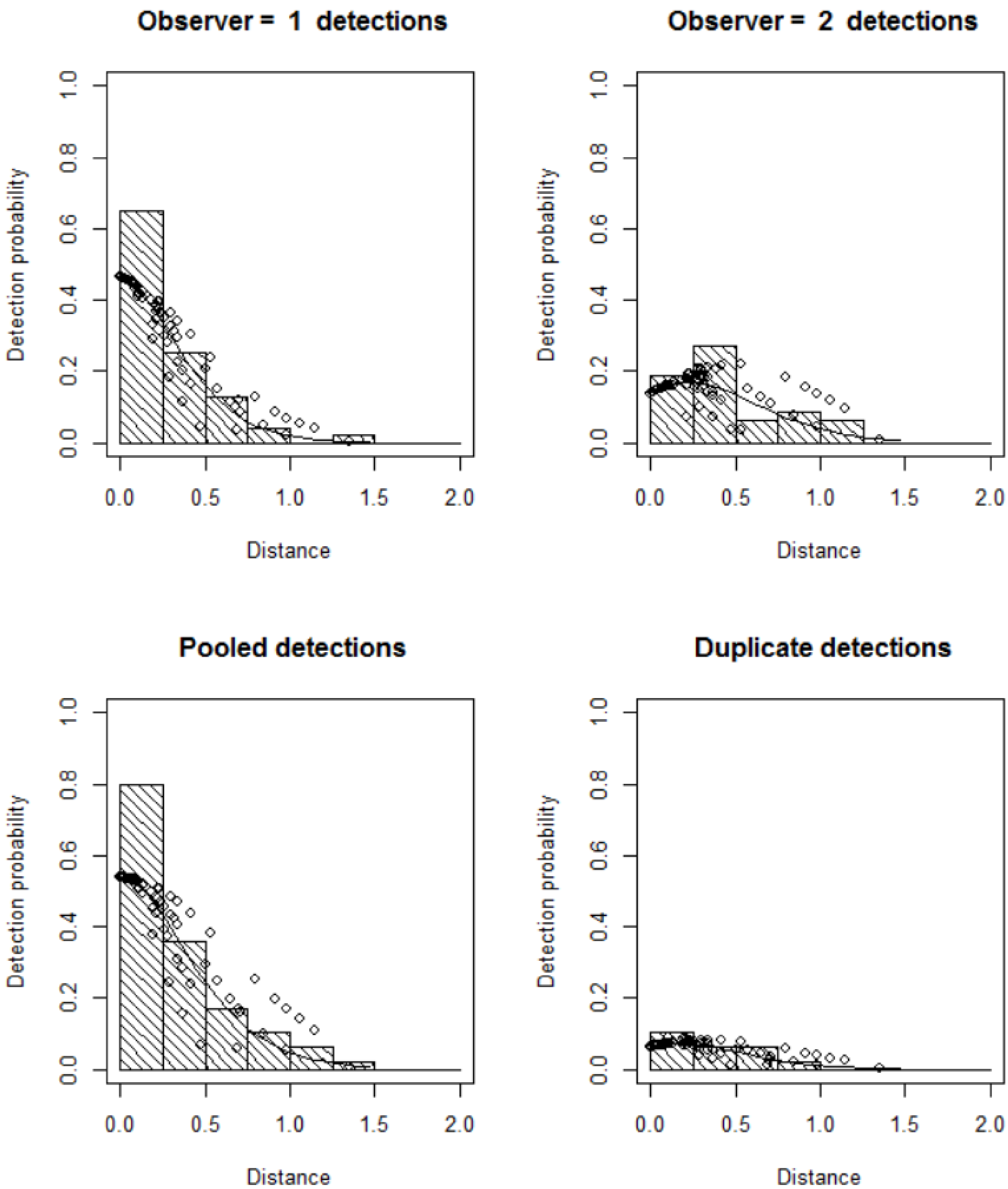

Figure 23. Detection probabilities for MRDS for Medium debris.

Absolute abundance estimates using corrections based on the detection function were 265 (± 180 95%CI) for medium, 336 (± 159 95%CI) for large, and 1031 (± 378 95%CI) for all size classes (Table 11-Table 13, Figure 24).

Table 11. Summary statistics of best fit MRDS models for all debris.

Debris Clusters							
Region	Area (km²)	Covered Area (km²)	Effort	n	Segments	Encounter Rate	CV
North	1127.28	1690.92	563.64	71	20	0.13	0.18
South	1130.78	1611.36	537.12	193	20	0.30	0.11
Total	2258.06	3302.28	1100.76	264	40	0.24	0.12
Density							
Region	Estimate	SE	CV	Lower Confidence Limit	Upper Confidence Limit	df	
North	0.23	0.06	0.24	0.15	0.39	49.71	
South	0.67	0.13	0.19	0.46	0.99	106.72	
Total	0.46	0.08	0.18	0.32	0.65	195.98	
Abundance							
Region	Estimate	SE	CV	Lower Confidence Limit	Upper Confidence Limit	df	
North	269.30	65.63	0.24	166.22	436.33	49.71	
South	762.34	148.49	0.19	520.00	1117.60	106.72	
Total	1031.65	189.44	0.18	720.37	1477.43	195.98	

Table 12. Summary statistics of best fit MRDS models for medium debris.

Debris Clusters							
Region	Area (km²)	Covered Area (km²)	Effort	n	Segments	Encounter Rate	CV
North	1127.28	1690.92	563.64	15	20	0.023	0.30
South	1130.78	1611.36	537.12	57	20	0.19	0.18
Total	2258.06	3302.28	1100.76	72	40	0.01	0.18
Density							
Region	Estimate	SE	CV	Lower Confidence Limit	Upper Confidence Limit	df	
North	0.04	0.17	0.41	0.02	0.09	55.40	
South	0.19	0.07	0.34	0.10	0.37	81.71	
Total	0.12	0.04	0.33	0.06	0.22	89.42	
Abundance							
Region	Estimate	SE	CV	Lower Confidence Limit	Upper Confidence Limit	df	
North	47.51	19.64	0.41	21.44	105.30	55.40	
South	217.42	74.52	0.34	112.03	421.93	81.71	
Total	265.93	87.06	0.33	140.22	500.55	89.42	

Table 13. Summary statistics of best fit MRDS models for large debris.

Debris Clusters							
Region	Area (km^2)	Covered Area (km^2)	Effort	n	Segments	Encounter Rate	CV
North	1127.28	1690.92	563.64	18	20	0.03	0.29
South	1130.78	1611.36	537.12	69	20	0.13	0.15
Total	2258.06	3302.28	1100.76	87	40	0.08	0.17
Density							
Region	Estimate	SE	CV	Lower Confidence Limit	Upper Confidence Limit	df	
North	0.06	0.02	0.38	0.03	0.13	30.72	
South	0.24	0.06	0.25	0.15	0.38	64.84	
Total	0.15	0.04	0.23	0.09	0.24	96.49	
Abundance							
Region	Estimate	SE	CV	Lower Confidence Limit	Upper Confidence Limit	df	
North	69.47	26.16	0.38	33.05	146.05	30.72	
South	266.92	65.56	0.25	164.61	432.82	64.84	
Total	336.40	78.38	0.23	213.13	530.94	96.49	

After correcting for the proportion of debris that were removed from MRCD analyses due to missing distances, these values were 336 (± 229 95%CI) for medium, 427 (± 202 95%CI) for large, and 1309 (± 480 95%CI) for debris of all size classes (Figure 10).

Overall, the estimated abundance of debris was greatest in the Southern most-transect (Transect 2), with more than double the debris estimated for the Northern-most transect (Transect 1). The western most region of Transect 2 had the greatest estimated debris abundance, with the eastern end of Transect 1 (approximately the last third of the transect) having greater estimated abundance than other areas of the transect (Figure 25, Figure 26).

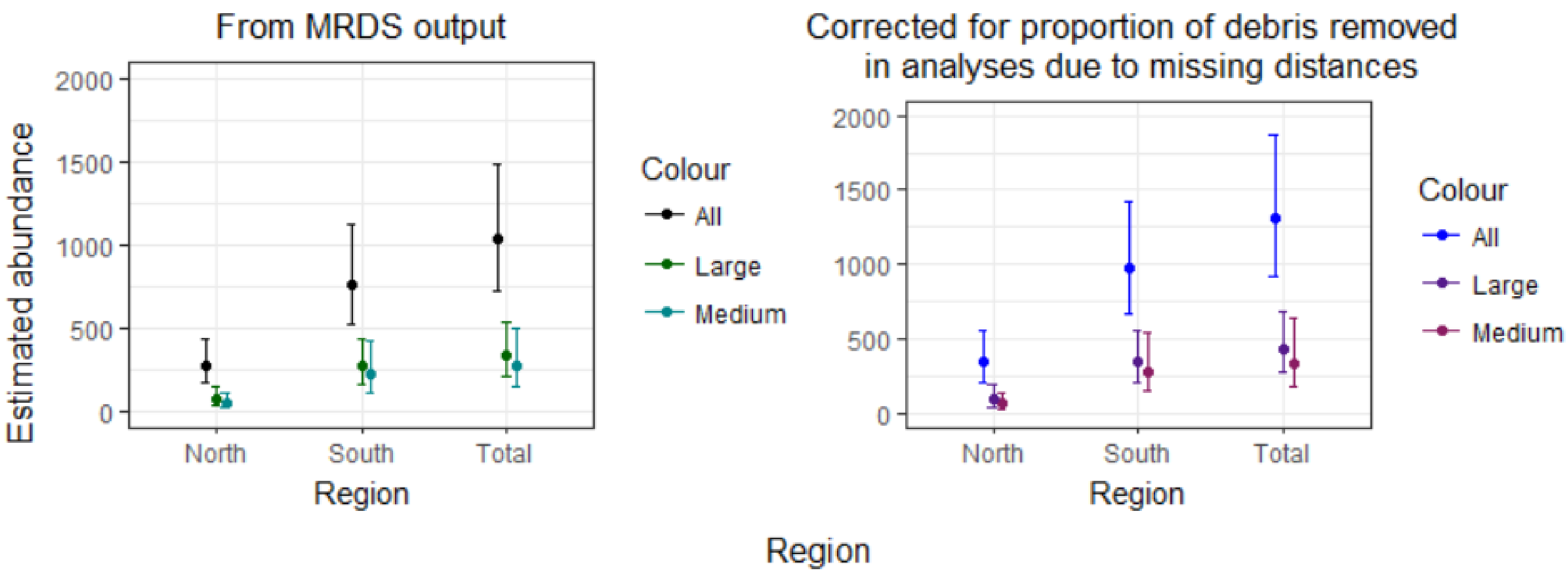

Figure 24. Estimated abundance (uncorrected from MRDS output and corrected for proportion of debris removed due to missing distances) of all, medium, and large debris within the South (Transect 1), North (Transect 2) and in both (Transects combined) based on the best MRDS models.

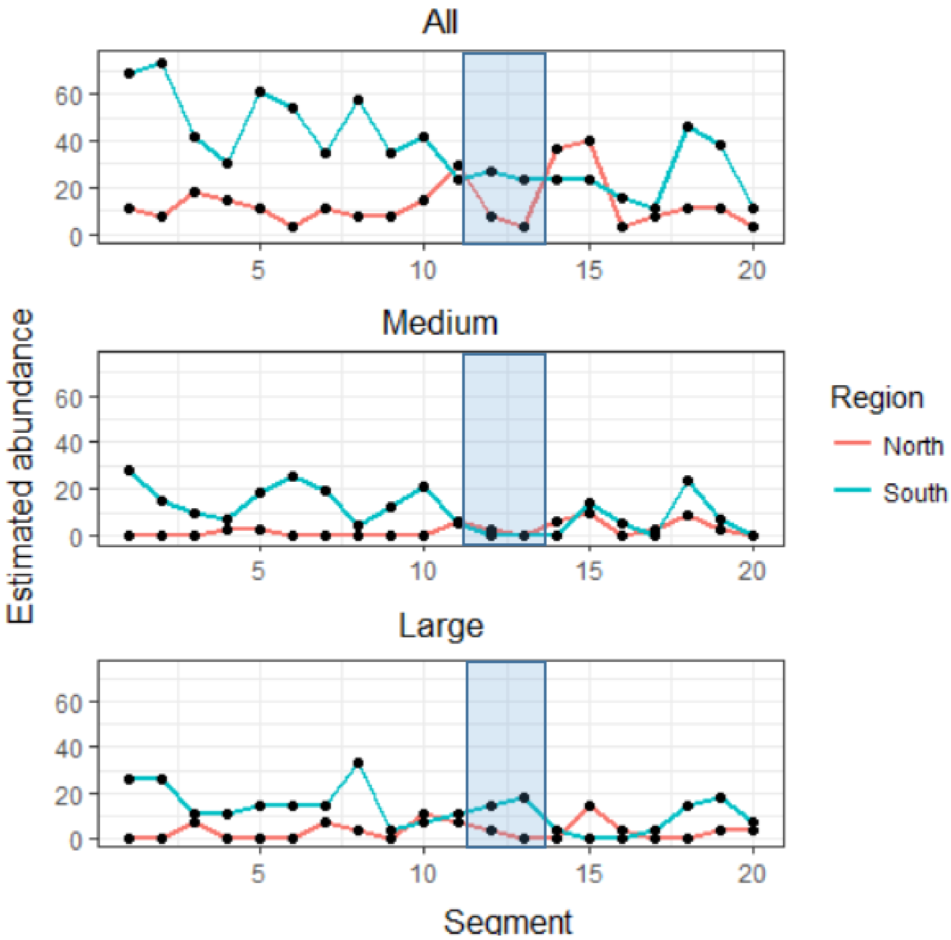

Figure 25. Estimated abundance of all, medium, and large debris within each transect segment based on the best MRDS models (shaded area corresponds with location of clouds below the aircraft in the Southern region).

Table 14. Estimated density of debris per linear km and per area for each segment.

Segment	Linear density (debris km^{-1})						Density (Debris km^{-2})					
	North			South			North			South		
	Total	Large	Medium	Total	Large	Medium	Total	Large	Medium	Total	Large	Medium
1	0.39	0.00	0.00	2.44	0.91	1.00	0.13	0.00	0.00	0.81	0.30	0.33
2	0.26	0.00	0.00	2.57	0.91	0.53	0.09	0.00	0.00	0.86	0.30	0.18
3	0.65	0.25	0.00	1.50	0.39	0.36	0.22	0.08	0.00	0.50	0.13	0.12
4	0.52	0.00	0.11	1.08	0.39	0.24	0.17	0.00	0.04	0.36	0.13	0.08
5	0.39	0.00	0.11	2.17	0.52	0.65	0.13	0.00	0.04	0.72	0.17	0.22
6	0.13	0.00	0.00	1.90	0.52	0.91	0.04	0.00	0.00	0.63	0.17	0.30
7	0.39	0.25	0.00	1.22	0.52	0.67	0.13	0.08	0.00	0.41	0.17	0.22
8	0.26	0.12	0.00	2.03	1.16	0.17	0.09	0.04	0.00	0.68	0.39	0.06
9	0.26	0.00	0.00	1.22	0.13	0.43	0.09	0.00	0.00	0.41	0.04	0.14
10	0.52	0.37	0.00	1.49	0.26	0.73	0.17	0.12	0.00	0.50	0.09	0.24
11	1.03	0.25	0.23	0.81	0.39	0.21	0.34	0.08	0.08	0.27	0.13	0.07
12	0.26	0.12	0.11	0.95	0.52	0.00	0.09	0.04	0.04	0.32	0.17	0.00
13	0.13	0.00	0.00	0.81	0.65	0.00	0.04	0.00	0.00	0.27	0.22	0.00
14	1.29	0.00	0.23	0.81	0.13	0.00	0.43	0.00	0.08	0.27	0.04	0.00
15	1.42	0.49	0.34	0.81	0.00	0.51	0.47	0.16	0.11	0.27	0.00	0.17
16	0.13	0.12	0.00	0.54	0.00	0.21	0.04	0.04	0.00	0.18	0.00	0.07
17	0.26	0.00	0.11	1.37	0.43	0.00	0.09	0.00	0.04	0.46	0.14	0.00
18	0.39	0.00	0.31	2.32	0.74	1.19	0.13	0.00	0.10	0.77	0.25	0.40
19	0.39	0.12	0.11	1.36	0.65	0.24	0.13	0.04	0.04	0.45	0.22	0.08
20	0.13	0.12	0.00	0.41	0.26	0.00	0.04	0.04	0.00	0.14	0.09	0.00

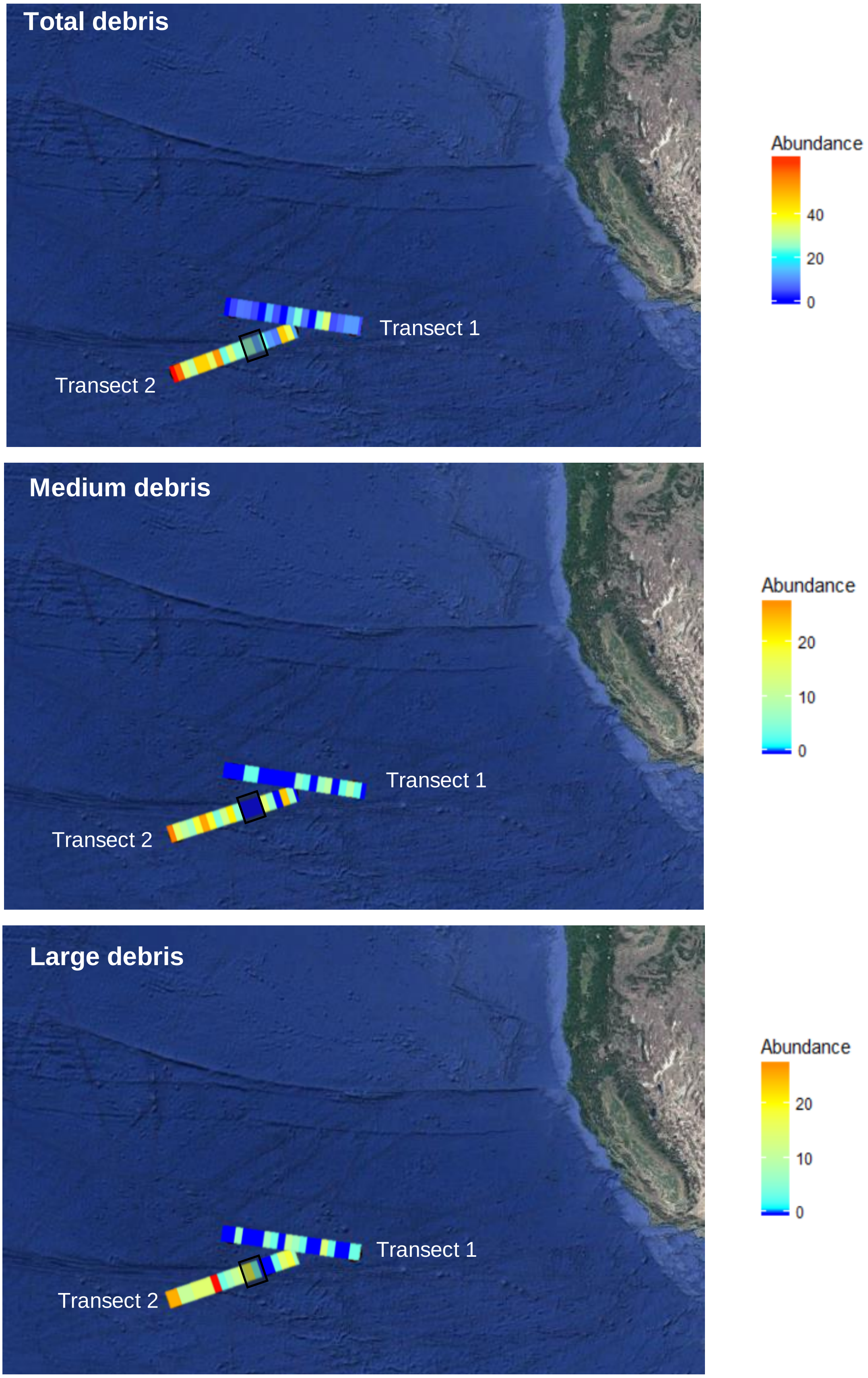

Figure 26. Heatmap of estimated abundance of total, medium and large debris along Transects 1 and 2 in the Pacific Ocean (Source of map: Google Earth; black box on Transect 2 is an area where low cloud cover was encountered that intermittently obscured the view below the aircraft).

While conditions did not have a consistent effect on abundance in the models, glare was intense on the starboard side of the aircraft and was identified as causing difficulty in observations by the observers. Thus, a 2-observer (port side only) and 4-observer models were run to compare results. Models including data from only the port side (2-observer model) resulted in consistently higher abundance estimates than 4-observer models (Table 15 and Figure 27), with a maximum of above 1.2 debris per km^2.

Table 15. Estimated density of debris per unit area for each segment resulting from a 4-observer and 2 observer models.

Density based on 4-observer model (Debris km^{-2})		Density based on 2-observer model (Debris km^{-2})	
North	South	North	South
0.13	0.81	0.07	1.21
0.09	0.86	0.15	0.88
0.22	0.50	0.23	0.64
0.17	0.36	0.23	0.56
0.13	0.72	0.15	0.64
0.04	0.63	0.00	0.80
0.13	0.41	0.23	0.56
0.09	0.68	0.07	0.72
0.09	0.41	0.07	0.32
0.17	0.50	0.23	0.80
0.34	0.27	0.46	0.32
0.09	0.32	0.15	0.48
0.04	0.27	0.07	0.32
0.43	0.27	0.69	0.24
0.47	0.27	0.77	0.40
0.04	0.18	0.07	0.32
0.09	0.46	0.15	0.81
0.13	0.77	0.23	1.14
0.13	0.45	0.23	0.40
0.04	0.14	0.07	0.24

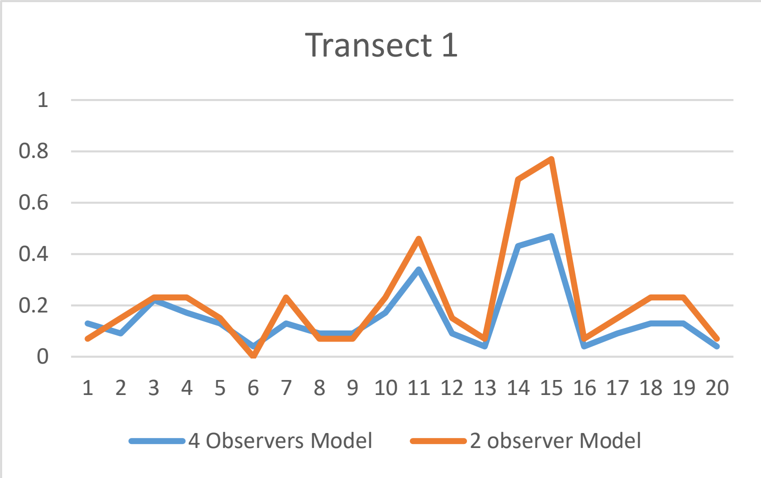

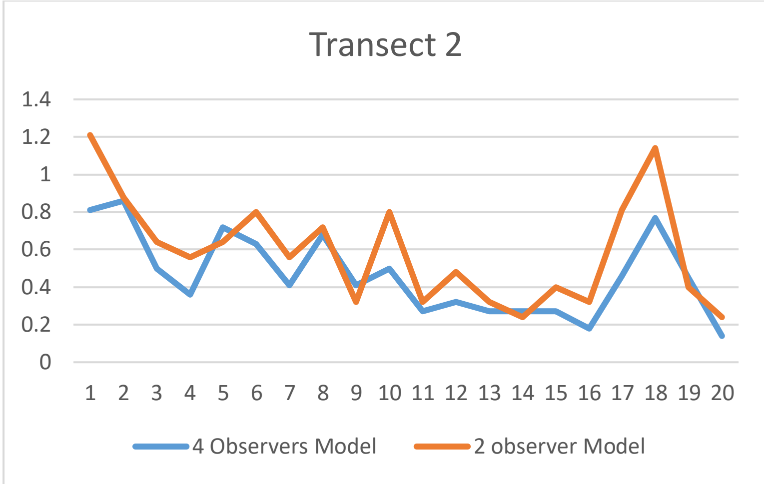

Figure 27. Estimated abundance of all, medium, and large debris within each transect segment based on the 2-observer and 4-observer models.

Discussion

The total estimated abundance of 1309 (± 480 95%CI) debris within 2258 km^2 (0.58 debris per km^2) is considered an underestimate of debris, as focus was placed on medium, large and huge debris size classes (debris larger than 0.5 m). There were many more small debris observed that were not recorded. These debris were in such high densities that it was impossible to manually record all of these using our visual observations method at the flying speed of 259.3 km hr^{-1} (140 knots).

Debris size classes were likely most accurate by measurements based on the photographs taken. Qualitative size classes were larger than those measured from photographs. A test flight for observers to train on known size objects at the designated flying height could have led to better size estimate results.

Based on measurements from photographs, medium (between 0.5 and 1 m in length) and large debris (1 to 5 m in length) made up 75% of the observations, with large debris recorded more often (43%) than medium size debris (32%). While many more small debris were observed than medium and large, these only made up 25% of recorded debris due to focus of visual observations on larger debris. Fewer than 1% were huge (> 5 m length). Correcting for detection probability, abundance of medium objects was estimated at 20% (266 objects), large at 28% (366 objects), and the rest of debris at 52%. These percentages could vary slightly with size correction for distortion of the objects resulting from the image not being taken perpendicular to the sea surface. While this was assumed to have a negligible effect on size class categorisation for the purposes of this report, there was a small effect estimated to be within approximately 20 cm. Future work can make a further correction for distortion.

Of the debris identified visually, the greatest percentage of debris type recorded were nets, followed by containers and other types outside the main categories, then by unknown objects and ropes. Debris types reported during visual observations and from inspecting photographs of the objects were mostly consistent. While visual inspection allows for observation of the behaviour of the object on the surface of the water, photographs allow for a careful inspection of the item, and a long-term record to be archived. In this survey expedition, because the flying speed and narrow doors only allowed a short period of observation akin to an instantaneious observation, and no circle-backs were included in the survey design (circling an item to confirm identification), photographs are likely to allow for more accurate identification. Based on photographs, 45% were nets, 11% ropes, 4% conbinations of nets, ropes, and floats, 3% floats, and 1% containers.

While there were large numbers of floats present, these were less frequently reported due to their smaller sizes and the focus of the work on medium, large and huge debris. The debris also varied in colour. However, the overwhelming majority of debris were white, with blue, green and grey debris following in number detected. All other colours generally were ‘washed’ out, presumably from being ‘bleached’ by the sun over time.

While MRDS estimates correct for imperfect detection as a function of range and observer perception bias, the methods assume detection at distance of 0 m from the aircraft (g(0)) to be perfect (probability = 1). The reality, is that at that flying height, smaller objects that have colours similar to the surrounding ocean were likely imperfectly detected even within close proximity to the aircraft. Thus, debris with attributes that make them more difficult to detect were almost certainly underestimated. These include debris type such as ropes in shape of a line (rather than tangled and more visible), debris relatively small in size, and light blue and grey debris. While debris type, size and colour were tested as covariates affecting detection with range, they did not fall out as significant.

In this report, abundance estimation and size class, debris type, and debris colour distributions from strip surveys have not been presented as they were undertaken as an addition to the original scope of work. However, comparative analyses using strip transect methods (both from photographs taken by observers as well as the fixed RGB sensor mounted on the aircraft) are recommended to inform best practices for future aerial surveys of ocean debris.

References

Buckland, S.T., D. R. Anderson, K.P. Burnham, J.L. Laake, D.L. Borchers, and L. Thomas eds. (2004). Advanced Distance Sampling, Oxford University Press, Oxford, UK.

Buckland, S.T., Rexstad, E.A., Marques, C.S., and Oedekoven, C.S. (2015). Distance sampling: methods and applications. Springer.

Burt, M.L., Borchers, D.L., Jenkins, K.J. and Marques, T.A. (2014). Using mark–recapture distance sampling methods on line transect surveys. Methods in Ecology and Evolution. Vol 5:1180–1191.

Laake, J.L. and Borchers, D. L. (2004). Methods for incomplete detection at distance zero. In Advanced Distance Sampling (S.T. Buckland, D.R. Anderson, K.P. Burnham, J.L. Laake, D.L. Borchers and L. Thomas, eds.). Pp 108-189. Oxford University Press, Oxford, U.K

Laake, J.L., D.L. Borchers, L. Thomas, D.L. Miller, *and* J.R.B. Bishop. (2015). mrds: Mark-Recapture Distance Sampling. R package version 2.1.14 ed. Available at: http://CRAN.R-project.org/package=mrds (accessed March 10, 2017).

Appendix A – Object ID Categories

Item	**Example Images**
Net	 
Rope	
Container	  
Buoy	  
Other	       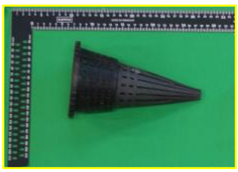

Appendix B – Beaufort Scale

Beaufort Scale	Description	Wind Speed	Wave Height (m)	Sea Conditions
0	Calm	Under 1km/h Under 1kn	0	Flat
1	Light air	1.1 – 5.5 km/h 1 – 2 kn	0 – 0.2	Ripples without crests.
2	Light winds	5.6 – 11 km/h 3 – 6 kn	0.2 – 0.5	Small wavelets. Crests of glassy appearance, not breaking.
3	Gentle winds	12 – 19 km/h 7 – 10 kn	0.5 – 1.0	Large wavelets. Crests begin to break, scattered white caps.
4	Moderate winds	20 – 28 km/h 11 – 15 kn	1 – 2	Small waves - becoming longer; fairly frequent white horses.
5	Fresh wins	30 – 39 km/h 16 – 20 kn	2 – 3	Moderate waves, taking a more pronounced long form; many white horses are formed - a chance of some spray
6	Strong winds	40 – 50 km/h 22 – 27 kn	3 – 4	Large waves begin to form; the white foam crests are more extensive with probably some spray
7	Near Gale	51 – 62 km/h 28 – 33 kn	4 – 5.5	Sea heaps up and white foam from breaking waves begins to be blown in streaks along direction of wind